JGR Atmospheres

RESEARCH ARTICLE

10.1029/2024JD042359

Look Within: Intraplume Differences on Smoke Aerosol Aging Driven by Concentration Gradients

Nicole A. June[1], Elizabeth B. Wiggins[2], Edward L. Winstead[2,3], Claire E. Robinson[2,3], K. Lee Thornhill[2,3], Kevin J. Sanchez[2], Richard H. Moore[2], Demetrios Pagonis[4], Hongyu Guo[5], Pedro Campuzano-Jost[5], Jose L. Jimenez[5,6], Taylor Shingler[2], Matthew M. Coggon[5,7], Jeff Peischl[5,7], Archana Dayalu[8], Marikate Mountain[8], Shantanu H. Jathar[9], Matthew J. Alvarado[8], and Jeffrey R. Pierce[1]

[1]Department of Atmospheric Science, Colorado State University, Fort Collins, CO, USA, [2]NASA Langley Research Center, Hampton, VA, USA, [3]Science Systems and Applications, Hampton, VA, USA, [4]Department of Chemistry and Biochemistry, Weber State University, Ogden, UT, USA, [5]Cooperative Institute for Research in Environmental Sciences, University of Colorado Boulder, Boulder, CO, USA, [6]Department of Chemistry, University of Colorado, Boulder, CO, USA, [7]NOAA Chemical Science Laboratory (CSL), Boulder, CO, USA, [8]Verisk Atmospheric and Environmental Research, Lexington, MA, USA, [9]Department of Mechanical Engineering, Colorado State University, Fort Collins, CO, USA

Key Points:

- A wildfire plume sampled during Fire Influence on Regional to Global Environments and Air Quality injected smoke simultaneously into the free troposphere (FT) and boundary layer
- We simulate the observed aerosol size and organic aerosol changes at the aircraft sampling altitude within the observational uncertainty
- Concentration and temperature gradients lead to differences in aerosol evolution between the FT and boundary layer

Supporting Information:

Supporting Information may be found in the online version of this article.

Correspondence to:

N. A. June and J. R. Pierce,
Nicole.June@colostate.edu;
Jeffrey.Pierce@colostate.edu

Citation:

June, N. A., Wiggins, E. B., Winstead, E. L., Robinson, C. E., Thornhill, K. L., Sanchez, K. J., et al. (2025). Look within: Intraplume differences on smoke aerosol aging driven by concentration gradients. *Journal of Geophysical Research: Atmospheres*, *130*, e2024JD042359. https://doi.org/10.1029/2024JD042359

Received 28 AUG 2024
Accepted 8 FEB 2025

Abstract

The evolution of organic aerosol (OA) composition and aerosol size distributions within smoke plumes are uncertain due to variability in the rates of OA evaporation/condensation and coagulation within a plume. It remains unclear how the evolution varies across different parts of individual plumes. We use a large eddy simulation model coupled with aerosol-microphysics and radiation models to simulate the Williams Flats fire sampled during the Fire Influence on Regional to Global Environments and Air Quality field campaign. At aircraft altitude, the model captures observed aerosol changes through 4 hr of aging. The model evolution of primary OA (POA), oxidized POA (OPOA), and secondary OA (SOA) shows that >90% of the SOA formation occurs before the first transect (~40 min of aging). Lidar observations and the model show a significant amount of smoke in the planetary boundary layer (PBL) and free troposphere (FT) with the model having equal amounts of smoke in the PBL and FT. Due to faster initial dilution, PBL concentrations are more than a factor of two lower than the FT concentrations, resulting in slower coagulational growth in the PBL. A 20 K temperature decrease with height in the PBL influences faster POA evaporation near the surface, while net OA evaporation in the FT is driven by continued dilution after the first aircraft transect. Net OA condensation in the PBL after the first transect is the result of areas with higher OH concentration leading to OPOA formation. Our results motivate the need for systematic observations of the vertical gradients of aerosol size and composition within smoke plumes.

Plain Language Summary

Wildfires are an important source of aerosol particles to the atmosphere. These aerosol particles are important for climate and human health. A 2019 field campaign flew an aircraft through wildfire smoke plumes in the western United States to take measurements of gasses and aerosol particles in the plume. We use these measurements and a high-resolution model to study the fine scale details of the evolution of the aerosol particles in the plume. In our case study, we find that there are differences in the evolution within the plume as a function of height due to temperature and concentration effects in the plume. These fine scale details have implications for large-scale air quality and climate models, which cannot resolve these plumes explicitly.

1. Introduction

Wildfires, which span orders of magnitude in size, are an important source of aerosol and gas-phase aerosol precursors to the atmosphere (Akagi et al., 2011; Andreae, 2019; Andreae & Merlet, 2001; Capes et al., 2008; Garofalo et al., 2019; Reid et al., 2005; Wiedinmyer et al., 2011). Biomass burning aerosol is predominantly in the accumulation mode (100–1,000 nm mode diameters) with a variable but often less abundant coarse mode (Adachi et al., 2022; Hodshire, Bian, et al., 2019; Janhäll et al., 2010; Reid et al., 2005). The submicron mass in wildfire smoke is predominantly (>90%) organic aerosol (OA) with additional minor contributions from black carbon and inorganic species (Bond et al., 2013; Capes et al., 2008; Carrico et al., 2008; Cubison et al., 2011; Garofalo et al., 2019; Hecobian et al., 2011; Mardi et al., 2018; Reid et al., 2005). This OA has been shown to impact the

Earth's radiative budget (Hobbs et al., 1997; Ramnarine et al., 2019), air quality (McClure et al., 2020; O'Dell et al., 2019; Schill et al., 2020; Yue et al., 2013), and human health (J. Chen et al., 2017; Ford et al., 2018; O'Dell et al., 2021) with aerosol size, composition, and abundance determining the magnitude of the effects (Kodros et al., 2018; Lee et al., 2013; Seinfeld & Pandis, 2016; Spracklen et al., 2011). However, uncertainties still remain surrounding OA emissions, evolution, and composition from wildfire smoke particularly in how these processes vary as a result of vertical and horizontal concentration gradients within smoke plumes.

Wildfires directly emit primary organic aerosol (POA), much of which is semivolatile and evaporates as smoke dilutes (Hatch et al., 2018; Huffman et al., 2009; May et al., 2013). The POA emissions from individual fires span orders of magnitude as a result of varying fire sizes, fuel types, and combustion properties (Bian et al., 2017; Gkatzelis et al., 2024; Hodshire, Akherati, et al., 2019; Hodshire, Bian, et al., 2019). Dilution rates of fires also tend to span orders of magnitude (Bian et al., 2017; Hodshire, Bian, et al., 2019). The dilution and emission variabilities as well as measurement uncertainties lead to high uncertainty in OA emission ratios used in models. Aircraft field campaigns tend to sample larger wildfires and often miss the first half-hour of aging due to flying risks, meaning there is still an observational gap in understanding evolution (Hodshire, Akherati, et al., 2019).

POA and the vapors in equilibrium with the POA (semivolatile organic compounds, SVOC) react to produce oxidized primary organic aerosol (OPOA), although some refer to this material as secondary organic aerosol (SOA) and reserve the term OPOA for that formed by particle-phase oxidation of POA (Dzepina et al., 2009; Hatch et al., 2018; Hennigan et al., 2010; Jen et al., 2019). Additionally, wildfires emit important OA precursor vapors with higher volatility, including oxygenated and non-oxygenated aromatics, heterocyclic organic compounds, and biogenic VOCs, which can oxidize in the atmosphere to form SOA (Gkatzelis et al., 2024; Hatch et al., 2015, 2017; Jathar et al., 2014; Koss et al., 2018; Palm et al., 2020; Sekimoto et al., 2018; Smith et al., 2014; Stockwell et al., 2015). Despite fires being a large source of VOCs to the atmosphere, the contribution of biomass burning to SOA/OPOA is uncertain (Granier et al., 2011; Lamarque et al., 2010; Reid et al., 2005; Shrivastava et al., 2017). Since the processes accounting for SOA and OPOA in models are typically parameterized due to uncertainties and computational limitations of simulating a large number of VOC species individually (Bilsback et al., 2023; Charan et al., 2019), the evolution of OPOA and SOA in wildfire smoke needs to be well understood to improve estimates of biomass burning on climate and health impacts.

Further complicating the understanding of OA, the evolution of the OA enhancement ratio (OAER; ΔOA/ΔCO) as smoke ages has been observed to either increase, decrease, or remain constant (Akagi et al., 2012; Cubison et al., 2011; Hecobian et al., 2011; Hobbs et al., 2003; Jolleys et al., 2015; May et al., 2015; Pagonis et al., 2023; Sakamoto et al., 2015; Vakkari et al., 2014; Yokelson et al., 2009; Zhou et al., 2017). The ΔOA/ΔCO corrects for dilution, showing the net change in OA as smoke ages due to the effects of POA evaporation and OPOA/SOA formation (Akagi et al., 2012). Field studies have suggested that OPOA/SOA condensation and POA evaporation balance each other in the wildfire plume leading to little net change in OA during the first few hours of aging (Akherati et al., 2022; Hodshire et al., 2021; Hodshire, Akherati, et al., 2019; May et al., 2015; Palm et al., 2020). This hypothesis was supported by simulations of wildfire plumes measured during the WE-CAN field campaign that showed dilution-driven evaporation of POA and simultaneous production of SOA explain the lack of change in OA enhancement ratios observed during the first 2–8 hr of physical aging (Akherati et al., 2022). At approximately 4 hr of aging, the OA in these plumes was 65% POA, 25% OPOA, and 10% SOA according to the simulations (Akherati et al., 2022). The variability in ΔOA/ΔCO evolution may also be influenced by the concentration of the plume (Bian et al., 2017; Hodshire et al., 2021; June et al., 2022). For example, plumes sampled during the Fire Influence on Regional to Global Environments and Air Quality (FIREX-AQ) campaign tended to have an observed ΔOA/ΔCO decrease in more concentrated plumes and an ΔOA/ΔCO increase in less concentrated plumes after the first transect (June et al., 2022; Pagonis et al., 2023). Prior to the first transect, there is observational evidence for rapid evaporation in less concentrated plumes evidenced by the ΔOA/ΔCO at the first transect tending to be lowest in the most dilute plumes sampled during FIREX-AQ (June et al., 2022).

Aerosol size distributions generally shift toward larger sizes as smoke ages, which is predominantly due to coagulation with slight impacts due to net condensation or evaporation of OA (Hodshire, Akherati, et al., 2019; June et al., 2022; Sakamoto et al., 2016). Coagulation reduces the particle number concentration, shifts the distribution to larger sizes, and narrows the modal width of the size distribution as a result of collisions resulting in faster loss of smaller particles, whereas the larger particles grow in size slightly (Hodshire, Akherati, et al., 2019; Janhäll et al., 2010; June et al., 2022; Sakamoto et al., 2016). Number median diameters have been observed to increase from 40 to 150 nm in fresh smoke (<1 hr aging) to 175–290 nm in smoke that has aged for 3–6 hr (Hodshire et al., 2021; Janhäll et al., 2010; June et al., 2022; Reid & Hobbs, 1998). The coagulation rate is proportional to the square of the number concentration (when the sizes are fixed), meaning that more concentrated plumes have more rapid coagulation (Seinfeld & Pandis, 2016). The dilution rate of the plume also has an impact, since a plume mixing into the clean background air at a slower rate will have a slower decrease in number concentration allowing for sustained coagulation (June et al., 2022; Sakamoto et al., 2016).

Within a single smoke plume, the processes driving aging can vary due to mixing and gradients in concentration (differences in concentrations in different regions of the plume) (Decker et al., 2021; Hodshire et al., 2021; June et al., 2022; Pagonis et al., 2023; Peng et al., 2020; Wang et al., 2021; Xu et al., 2021). Studies using observational data from the Biomass Burning Observation Project and FIREX-AQ have shown there to be differences in coagulation and net OA evaporation/condensation between the edge and core of a plume (Hodshire et al., 2021; June et al., 2022). June et al. (2022) found faster coagulation and faster evaporation in the concentrated centers of plumes sampled during FIREX-AQ; however, there was also evidence of rapid changes in ΔOA/ΔCO before the first transect. Studies examining the composition of ΔOA/ΔCO evolution specifically looking at POA, OPOA, and SOA in smoke plumes have often focused on either the plume average at the altitude of an aircraft or horizontal crosswind variability at that altitude (Akherati et al., 2022; Hodshire et al., 2021; June et al., 2022; Palm et al., 2020, 2021). There is less understanding of how smoke ages at varying heights in a smoke plume, and improving this understanding would be beneficial to understanding impacts on air quality at the surface and aloft (Pagonis et al., 2023). Pagonis et al. (2023) compared ΔOA/ΔCO measurements from recent field campaigns sampled at aircraft altitude and in smoke plumes sampled at the ground, finding that the ground measurements had an ΔOA/ΔCO a third of that at the aircraft measurements. These findings are explained by temperature differences: at aircraft altitude (270 K) the SVOC favor the particle phase, whereas the surface (310 K) SVOC partitioning favors the gas phase (Pagonis et al., 2023). For example, the Sheridan Fire sampled under a range of temperatures during FIREX-AQ showed a decrease in ΔOA/ΔCO with increasing temperature consistent with the plume-by-plume analysis (Pagonis et al., 2023). The vertical variances in plume evolution are likely influenced by the initial smoke injection height and environmental conditions that a plume is emitted into, such as a deep planetary boundary layer (PBL) versus a shallow one or into the free troposphere (FT). Despite recent field campaigns improving the sampling of smoke plumes and the gradients within them, studies have typically focused on plume average evolution and variability in evolution at a single height. Additionally, understanding the evolution of smoke prior to the first transect remains an ongoing field of research.

Simulations of heterogeneity within smoke plumes has been done before with models such as system for atmospheric modeling coupled to the aerosol simulation program (SAM-ASP) (Lonsdale et al., 2020), WRF-LES-Chemistry (Wang et al., 2021), SAM-TOMAS (Sakamoto et al., 2016), CRM6 (Alvarado & Prinn, 2009). Lonsdale et al. (2020) used the SAM-ASP 2D Lagrangian model to simulate gas and aerosol chemistry in a wildfire smoke plume. Although the model showed strong intraplume gradients in CO, gradients were less pronounced in OA and O_3 due to the impact of the plume not being included in the photolysis rates. Additionally, this study did not include evaluation of simulated aerosol size distributions due to a lack of measurements (Lonsdale et al., 2020). Wang et al. (2021) examined ozone and NO_x chemistry using a large eddy simulation (LES) of a plume sampled during FIREX-AQ in the WRF-LES-Chemistry model. They found chemistry to be suppressed at the center of the plume as well as below the concentrated free tropospheric plume (Wang et al., 2021). This study did not include analysis of OA or aerosol size distributions.

In this study, we use a 2D Lagrangian model (SAM-ASP) coupled with the tropospheric ultraviolet and visible (TUV) model to further the understanding of vertical variability of OA and aerosol size distributions in near-term (first 4 hr) aging of a wildfire plume sampled during FIREX-AQ that had emissions into both the FT and PBL. In Section 2, we describe the observational data and model setup. In Section 3, we first analyze the model performance against observations at the aircraft altitude. We then analyze the impacts of in-plume concentration gradients on differences in aging between the boundary layer and FT.

2. Materials and Methods

2.1. FIREX-AQ Field Campaign Data

The FIREX-AQ campaign sampled wildfire smoke in the western United States in July–August 2019 (Warneke et al., 2023). In our study, we use data from the first sampling of the Williams Flats Fire around 22 UTC on 3

August 2019. It should be noted that the aircraft moved downwind 4 times faster than the smoke, meaning that the smoke sampled farther from the fire generally had been emitted by the fire earlier in the day than the smoke sampled close to the fire. For this reason, transects used for model-observation comparison are limited to those identified as the most Lagrangian: transects in the vertically densest section of the plume as identified by lidar measurements with fairly consistent modified combustion efficiency (0.89–0.92) suggesting relatively constant burning conditions (June et al., 2022; Wang et al., 2021). Additionally, we also limit our analysis to the first 4 hr of physical aging due to the limits of the pseudo-Lagrangian sampling pattern (aircraft moving downwind faster than the plume). The FIREX-AQ campaign also included a mobile laboratory truck; however, for this day and fire, the analysis measurements of aerosol size smaller than 500 nm and aerosol mass spectrometer (AMS) measurements are not available.

The TSI laser aerosol spectrometer (LAS) measured the aerosol size distribution between 0.1 and 5 μm at 1 Hz resolution (Moore et al., 2021). The LAS uses a helium-neon laser to detect particles across this size range with 20% uncertainty across all sizes. The LAS was calibrated using size-classified ammonium sulfate aerosols. More detailed information on the LAS calibration and performance during FIREX-AQ can be found in the work of Moore et al. (2021). As described by June et al. (2022), we apply corrections to the LAS measurements for evaporation due to heating in the sampling lines and optical saturation of the LAS sensor.

The Aerodyne high-resolution time-of-flight AMS measured OA at 1 or 5 Hz resolution (Pagonis et al., 2021; Warneke et al., 2023). The uncertainty for OA measured by the AMS has been estimated to be 38% (2 sigma) mostly due to uncertainties in collection efficiency and the relative ionization energy of OA (Bahreini et al., 2005, 2009; Guo et al., 2021). An evaporation correction is applied to the AMS measurements to account for evaporation due to heating in the sampling lines (Pagonis et al., 2023).

The NASA Langley Research Center's airborne Differential Absorption Lidar and High Spectral Resolution Lidar (DIAL-HSRL) provides measurements of 180-degree aerosol backscatter at 532 nm. Here, it is used to provide qualitative comparisons to the model of the vertical distribution of aerosol particles throughout the smoke plume.

Gas phase measurements include CO, O_3, NO_x as well as photolysis rates. CO was measured by the NOAA LGR at 5 Hz resolution and averaged to 1 Hz. The instrument operated with 2% uncertainty during FIREX-AQ (Bourgeois et al., 2022). The O_3 and NO_x measurements were made by the NOAA NO_yO_3 4-channel chemiluminescence instrument (Ryerson et al., 2000). The photolysis frequencies were measured by the NCAR CCD Actinic Flux Spectroradiometers (CAFS) instrument (Shetter & Müller, 1999).

2.2. SAM-ASP-TUV Model

We use a version of the SAM-ASP model now coupled with the TUV model. Lonsdale et al. (2020) introduces the coupling of SAM v6.10 to ASP v2.1; here, we briefly describe the details. In SAM-ASP, SAM is the LES component that is configured as a moving, 2D Lagrangian wall, oriented perpendicular to the mean wind in the layer of smoke injection (1,320–2,200 m). Due to the use of the mean wind, one limitation of the model is the inability to capture differences in physical age that occur between the edge and core of the plume as well as between the FT and PBL. The grid boxes in the 2D moving wall have a 500 × 500 m horizontal resolution with the total domain width being 120 km in the perpendicular to the wind direction (and 500 m in the with-wind direction). The vertical resolution is 40 m with a total vertical extent of 3.2 km. One limitation of the model is that it does not include the topography. We acknowledge that this means the model may have biases in turbulence due to the roll of terrain on boundary layer dynamics; however, prior studies have shown that these simulations with no terrain can be valuable in understanding the evolution seen in smoke plumes (Lonsdale et al., 2020; Wang et al., 2021). The meteorological conditions used in the model use the 3 hr, 32 km resolution North American Regional Reanalysis from the time of the flight (3 August 2019, 21:00 UTC to 4 August 2019, 00:00 UTC). SAM allows various configurations for the advection scheme, turbulence parameterization, radiation and cloud microphysics. Here, the configuration used is as described by Lonsdale et al. (2020), including the use of a positive definite monotonic advection scheme with a nonoscillatory option, the 1.5-order turbulent kinetic energy closure for subgrid-scale turbulence, and the cloud microphysics scheme of Morrison et al. (2005) (although clouds are not predicted nor were observed in the domain on our investigated day). Initial turbulence in the model is spun up for 3 hr using a warm bubble to allow for repeatable turbulence between sensitivity simulations. The turbulence is nudged to the reanalysis fields on a timescale of 3 hr. SAM transports all of the gas-phase and aerosol species calculated by ASP (Lonsdale et al., 2020). ASP is used to simulate the chemical and physical aging of biomass-burning plumes (Alvarado & Prinn, 2009; Alvarado et al., 2015). A sectional aerosol size distribution with 10 bins (0.025 to >1 μm) is used to represent the aerosol size distribution in ASP, which also includes inorganic and OA thermodynamics, condensation and evaporation, coagulation of aerosol particles, and aerosol optical properties (Alvarado et al., 2016).

In this version of SAM-ASP-TUV, we couple SAM-ASP v1.0 to the TUV model (Bais et al., 2003; Lonsdale et al., 2020). The coupling of SAM-ASP to TUV allows for online calculations of photolysis rates including the impact of aerosols. Aerosol optical depth, single scattering, and asymmetry parameter are sent from SAM-ASP to TUV. Tropospheric ultraviolet and visible predicts the photolysis rates across each column for 48 reactions (Table S1 in Supporting Information S1), which are sent back to ASP for chemistry.

We made updates to the SAM-ASP-TUV representation of OA chemistry to better represent SOA precursors and processes from recent field campaigns and modeling studies of wildfire plumes. The previous version of SAM-ASP used nine volatility bins spanning from saturation concentrations (C*) of 10^{-2} to 10^{6} μg m^{-3} at 298 K (each bin covering 1 order of magnitude) tracking POA, OPOA, and SOA together. To track POA/OPOA and SOA separately in our simulations, without adding additional species, we use four volatility bins (each covering 2 orders of magnitude) from 10^{-2} to 10^{6} μg m^{-3} for POA/OPOA and a second set of four volatility bins from 10^{-2} to 10^{6} μg m^{-3} for SOA. POA emissions are split into the 4 POA/OPOA volatility bins as shown in Figure S1 in Supporting Information S1 (Akherati et al., 2020, 2022; Bilsback et al., 2023; May et al., 2013). This range of C* bins spans from low-volatile organic compounds to intermediate-volatile organic compounds. For POA/OPOA, these C* have previously been shown to be the range observed in fresh wildfire smoke (Bian et al., 2017; Hatch et al., 2017; May et al., 2013). Using the configuration described here allows the POA/OPOA bins to have the same spacing and C* as the SOA bins for which we have updated information for the SOA processes in smoke. Kinetic partitioning is used to determine the amount of organics in the particle/gas phase in each of these bins. Based on Shrivastava et al. (2024), we use a reduced scheme for SOA precursors using two lumped precursor classes: OXARO and OTHER. OXARO represents all oxygenated aromatic precursors and OTHER represents all remaining SOA precursors including heterocyclics, aromatic hydrocarbons, biogenics, and acyclic VOCs (Shrivastava et al., 2024). The use of these two SOA precursor classes was based on previous biomass burning work (Akherati et al., 2020, 2022; Bilsback et al., 2023), which showed that these precursor classes can capture the majority of the SOA potential in wildfire plumes. The sum of OXARO and OTHER represents the total amount of SOA precursors in our simulations ($\mathrm{SOA_{Pre}}$). OXARO and OTHER each react with OH into the SOA volatility bins with yields and reaction rates shown in Figure S1 in Supporting Information S1 (Shrivastava et al., 2024). Once SOA products are in the volatility bins, they do not react with OH to change volatility after formation; the parameterized volatilities already include multi-general aging representative of the first several hours in the plume.

Since OPOA is not tracked explicitly, we run five simulations with different POA/OPOA aging schemes (Table S2 in Supporting Information S1). A no-aging case, where the POA/OPOA volatility bins do not react with OH, is used to estimate the OPOA fraction in the other four simulations using the difference between POA between a simulation with an aging scheme and the no-aging case. For the simulations with POA aging, the POA/OPOA volatility bins react with OH to form lower-volatile VOC and higher-volatile VOC. The total yield of these reactions is 1.075 based on Robinson et al. (2007) and Ahmadov et al. (2012). Each sensitivity simulation tests a different fraction of fragmentation from 0% to 50% (Table S2 in Supporting Information S1). All of the POA aging scheme simulations are run twice, once with a base case SOA precursor emission rate and once with a doubling of the SOA precursor emission rate. We primarily discuss results for the configuration with the base case $\mathrm{SOA_{Pre}}$ emissions with the POA following the 0.825 functionalization mass yield and 0.25 fragmentation mass yield. However, we also discuss the sensitivity of model-observation agreement due to the assumptions made for OA aging.

Emissions to SAM-ASP-TUV occur after turbulence spin-up over a time period of 1 hr while the 2D wall passes over the fire area. During this hour chemistry does not happen in the plume but mixing occurs. Emissions ratios, initial CO, and aerosol size distribution initial conditions are determined following the methodology of Lonsdale et al. (2020). Some emissions ratios were updated using the Gkatzelis et al. (2024) study, which gives emission ratios and emission factors for US wildfires based on FIREX-AQ measurements. Emissions ratios for the SOA precursor classes, OXARO and OTHER, are from Shrivastava et al. (2024). A scaling factor is used to adjust total emissions in order to yield agreement in CO, OA, and total aerosol number concentration at the time of the first transect. Although the emissions ratios used are consistent with estimates for western US wildfires, the process of adjusting to match the model and observations at the first transect likely impacts our conclusions on processes prior to the first transect where there is no observational constraint. The emitted aerosol median diameter and modal width, 110 nm and 1.5, respectively, was selected to yield agreement in modeled and observed diameter at the first transect assuming a lognormal mode. This selection was done through an iterative process of adjusting emitted aerosol median diameter and modal width within the range of prior studies (e.g., Grieshop et al., 2009) until there was a match in the median diameter at the first transect. Other than the SOA precursor emission rate, which is adjusted for some sensitivity simulations, all emissions are fixed between the sensitivity simulations.

2.3. Derived Quantities

In the observations, flags provided in the FIREX-AQ data set are used to determine measurements in background air and in-plume. The enhancement of species *X* due to the presence of smoke (ΔX) is determined by subtracting the average background concentration ($X_{\text{background}}$) from the in-plume concentration (X_{inplume}). The minimum observed ΔCO was 135 ppbv. For the model, we use ΔCO greater than 135 ppbv as the threshold for determining if a model grid box is considered in-plume. Enhancement ratios (ΔX/ΔCO) are used to evaluate the dilution-corrected evolution of a species. Lastly, averages within the plume are concentration weighted such that the more concentrated parts of the plume contribute more to the averaged quantity.

For the observations, the number median diameter (D_{pm}) and number concentration (N) are calculated using the same methodology as June et al. (2022) by fitting a lognormal distribution from 50 nm to 2 μm to the binned dN/dlogD_p measurements from the LAS. A single mode is enough to describe the size distributions sampled in this plume (June et al., 2022; Moore et al., 2021). For the model, the N and D_{pm} are calculated using the same methodology as for the model output also limiting the model to the size ranges from 50 nm to 2 μm. In the 4 hr of aging used in our study, few particles in the model and observations grow outside of this size range.

For model evaluation against the DIAL-HSRL observations, we calculate an estimate of the backscatter at 532 nm. We use Mie Code to calculate the backscatter at 532 nm (Bohren & Huffman, 2008). We use an assumed ambient particle refractive index (1.47 + 0.007i) in our backscatter calculations based on Moore et al. (2021), which calculated refractive indices for different FIREX-AQ plumes. Although this assumption for a refractive index introduces some uncertainties, it allows for a qualitative comparison of the vertical distribution of the modeled and observed plume.

We additionally define a quantity of $\Delta\text{CO}_{\text{loading}}$ to understand the total amount of smoke in the PBL and FT for any vertical/cross wind cross section of the plume (Equation 1).

$$\Delta\text{CO}_{\text{Loading}} = \sum_{z}\sum_{x} \Delta\text{CO}_{\frac{\mu g}{m^3},\text{box}}\, \Delta z_{\text{grid}}\, \Delta x_{\text{grid}}\, U_{\text{wall}} \tag{1}$$

where Δz_{grid} is equal to 40 m, Δx_{grid} is equal to 500 m, and U_{wall} is equal to the speed that the 2D Lagrangian wall is advected downwind. We sum over the entire plume, the plume in the PBL, and the plume in the FT to determine the fraction of $\Delta\text{CO}_{\text{loading}}$ in the FT and the PBL. We use a PBL height of 1,880 m above ground level (AGL) based on the reanalysis meteorology vertical profiles of temperature used in the model and the height to which ΔCO is well mixed in the model after 1 hr of aging. The plume above this height is considered to be FT. In reality, the PBL height likely evolves slightly during our 4 hr simulation, but given that the aircraft samples the plane in about 2 hr, these effects would be difficult to disentangle from other observational uncertainties. This quantity is not directly input into the model and does not influence the model output; it is used to aid in interpretation of the model results. The model is rather spinning up turbulence and creating a PBL like environment and being nudged to the reanalysis on 3 hr timescales.

3. Results

3.1. Model-Observation Comparisons

Both the DIAL-HSRL observations (Figures 1a–1c) and the model (Figures 1d–1f) backscatter at 532 nm show a plume located in the FT and in the PBL. We have not removed the background backscatter from either the

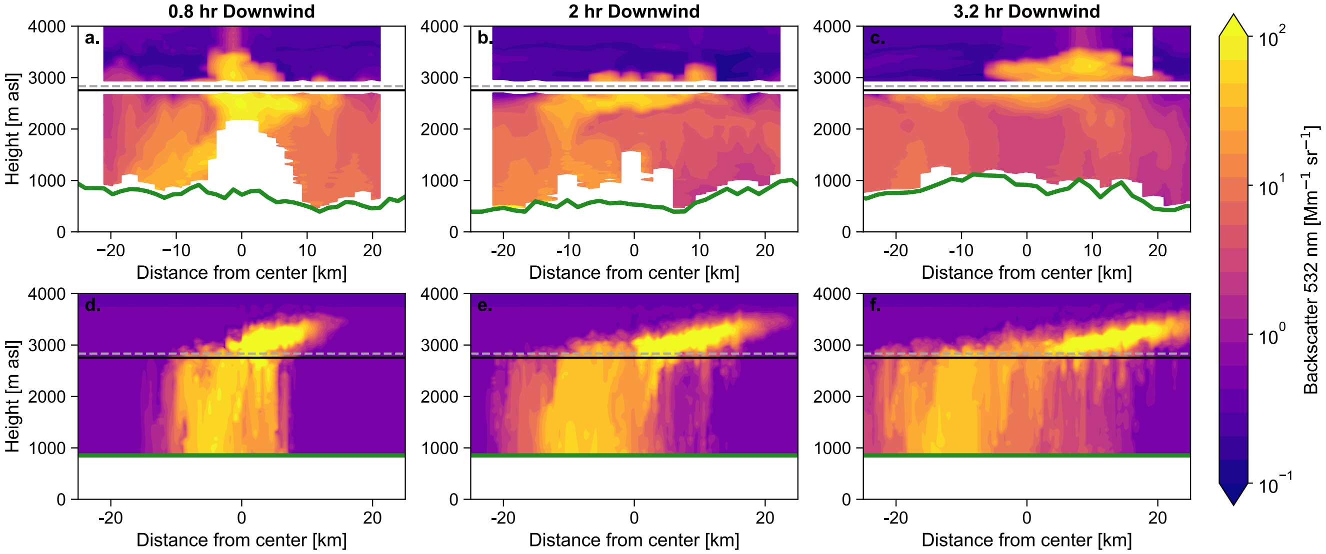

Figure 1. (a)–(c) Observed Differential Absorption Lidar and High Spectral Resolution Lidar backscatter at 532 nm for three transects observed during the 3 August 2019 sampling of the Williams Flats Fire. (d)–(f) The corresponding backscatter at 532 nm for the SAM-ASP-TUV model. Note that the alignment horizontally between the top and bottom rows may differ as the center in panels (a)–(c) is based on the time it took the aircraft to complete the transect, whereas the center in panels (d)–(f) is the center of the model. In the observed panels, there are areas of white where data are not reported at the altitude of the aircraft as well as topography effects near the surface or from in-plume attenuation. Topography is not included in the model. The vertical axes limits are set such that the vertical extent is approximately equal between the model and observation in units of m above sea level (m asl). The solid black horizontal line is the height of the planetary boundary layer determined from the reanalysis used in the model. The dashed gray line is the height of the aircraft that sampled the plume. The ground altitude is plotted in green.

observations or the model. Therefore, there are horizontal discrepancies outside of the plume due to the model having an assumed constant background everywhere. On the observation panels (1a-c), there is a level of white where data are not reported for approximately 500 m around the aircraft level. Additionally, data are not reported when attenuation in the plume is too large or near the surface due to the impacts of the ground. Data not being reported due to plume attenuation are the primary cause of missing data in 1a and 1b, whereas 1c is more affected by the terrain. Our model does not include topography and therefore cannot represent these topographical features. The mixing to the surface pattern is similar to that shown for the same sampling of the Williams Flats Fire simulated with WRF-LES by Wang et al. (2021). At the time of the first transect (Figures 1a and 1d), the plume has yet to disperse much horizontally but has mixed to the surface in both the model and observation. After 2 hr of aging (Figures 1b and 1e), the free tropospheric plume has dispersed horizontally with one side of the plume showing stronger mixing to the surface due to the Ekman spiral (Wallace & Hobbs, 2006). At 2 hr, the model has the most concentrated part of the plume just above the aircraft, whereas the observations suggest that the aircraft sampled directly at the most concentrated part of the plume. At 3.2 hr of aging (Figures 1c and 1f), both the model and observations continue to show a free tropospheric plume and stronger mixing on one side of the plume to the surface. At this time, both the model and observations have a concentrated smoke layer above the aircraft. Although there is generally qualitative agreement between the DIAL-HSRL and the simulated backscatter, there are some discrepancies potentially due to both the pseudo-Lagrangian sampling and topographical effects on dispersion and PBL dynamics. Differences between the model and observations in terms of the amount of entrainment that occurs between the FT and the PBL could exist as a result of the observational limitation of pseudo-Lagrangian sampling and the model limitation of not including topography. However, without truly lagrangian observations, we cannot quantify how much of the model biases are due to lacking terrain or potential biases in turbulence. Although not a direct comparison, these backscatter comparisons suggest that the SAM-ASP-TUV qualitatively represents both the horizontal and vertical dispersion of the plume in the near-term aging.

The aircraft only sampled the free tropospheric portion of the plume, so our quantitative model evaluation (Figure 2) is for this portion of the plume only. The model captures the observed CO concentration dilution rate at the altitude of the aircraft and ΔCO concentrations throughout the first 4 hr of aging. Although there are higher ΔCO values just above the aircraft (blue lines) and lower ΔCO values just below (green lines) (Figure 2a). The

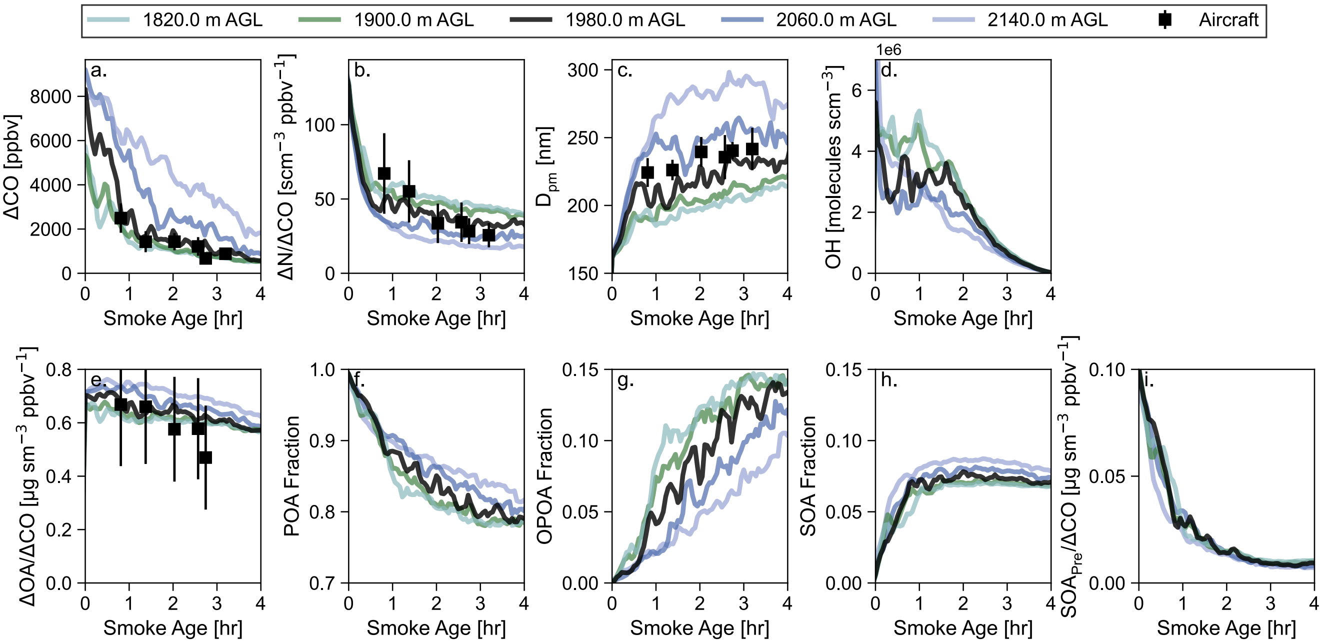

Figure 2. The transect average evolution of (a) ΔCO, (b) ΔN/ΔCO, (c) D_{pm}, (d) OH, (e) ΔOA/ΔCO, (f) primary organic aerosol fraction, (g) oxidized primary organic aerosol fraction, (h) secondary organic aerosol fraction, and (i) SOA pre/ΔCO. The solid-colored lines are the model plume average at five heights with the 1,980.0 m above ground level line being the altitude closest to the height of the aircraft. The transect-average aircraft observations for the 3 August 2019 sampling of the Williams Flats Fire are shown as black squares for panels (a)–(d) with the error bars showing the standard deviation of the measurements.

model representation of dilution at the aircraft altitude gives further confidence (beyond the DIAL-HSRL comparisons) that the model represents the dispersion of the plume.

The model generally captures the evolution of the plume average ΔN/ΔCO (Figure 2b) and D_{pm} (Figure 2c) measured by the aircraft within the variability of the transect. There are sensitivities to the altitude of comparison with faster coagulation above the aircraft and slower coagulation below. Prior to the first transect, the changes in ΔN/ΔCO and D_{pm} are due to rapid coagulation resulting in a factor-of-3 drop in number and a 30%–50% increase in D_{pm}. After 1 hr of aging, the coagulation rate slows as seen by the slower rate of decrease in ΔN/ΔCO. The slower increase in D_{pm} after 1 hr of aging is due to the slower coagulation rate; however, there are minor effects of evaporation due to the net decrease in ΔOA/ΔCO. The net decrease in ΔOA/ΔCO results in approximately 5% smaller particles at 4 hr of aging compared to if there was no net change in ΔOA/ΔCO (Figure S2 in Supporting Information S1).

The model and observations suggest net OA evaporation with a decrease in ΔOA/ΔCO from 0.7 to 0.58 μg sm^{-3} ppb^{-1} at approximately 3 hr of aging (Figure 2e). The final observation transect has a lower ΔOA/ΔCO than the model; however, this point does not follow the trend of the prior observation transects. In the model levels surrounding the aircraft, there are only slight impacts of the altitude on the ΔOA/ΔCO comparison. However, the comparisons reveal that the more concentrated levels above (2,060–2,140 m) had faster evaporation than the layers below (1,820–1,900 m) likely due to effects of there being more semivolatile OA to evaporate at higher concentrations. The OA evaporation primarily occurs in the C*(298 K) 10^4 μg m^{-3} bin with some evaporation in the C*(298 K) 10^2 μg m^{-3} bin (Figure S3 in Supporting Information S1). The evaporation in the volatility bin space is consistent with the approximately 280 K temperature at the aircraft altitude and the modeled ΔOA concentrations decreasing from 5,870 to 607 μg sm^{-3} at 3.2 hr. The reduction in ΔOA/ΔCO is the result of POA evaporation being greater than the increases in OPOA and SOA (Figures 2e–2h). We acknowledge that there is likely some uncertainty induced by the selection of volatility bins used in the model. However, given the consistency with observations at the aircraft altitude and the volatility bin setup being consistent with recent studies (e.g., Bian et al., 2017; Bilsback et al., 2023), we believe the setup used here to be reasonable within the uncertainties of current knowledge. After 4 hr of aging, the combined fraction of OPOA and SOA is about 21%, which is similar to the fractions of OPOA and SOA seen in simulations of wildfire plumes sampled during the WE-CAN field campaign (Akherati et al., 2022). The increases in SOA and OPOA are largest prior to the first transect (0.8 hr); after that point in time the SOA fraction remains approximately constant, whereas the OPOA continues to increase. The SOA fraction stops increasing due to the lack of SOA precursors remaining in the plume after 1 hr of aging (Figure 2i). The rapid changes in ΔOA/ΔCO before first measurement are consistent with prior studies, which have suggested the need to understand processes controlling the evolution in the first half hour of wildfire aging (Akherati et al., 2022; Bian et al., 2017; Cubison et al., 2011; Hodshire, Akherati, et al., 2019).

The OA aging sensitivity simulations (Table S2 in Supporting Information S1) all show net OA evaporation in agreement with the observations (Figure S4 in Supporting Information S1); however, there are minor impacts on ΔOA/ΔCO and D_{pm} observation agreement as well as the amounts of OPOA and SOA (Figure S4 in Supporting Information S1). For the scenarios with 2 × SOA_{Pre} emissions, the main difference is ΔOA/ΔCO is higher at all times relative to the 1 × SOA_{Pre} emissions due to the increase in SOA_{Pre} increasing the amount of SOA formed in the first hour of aging. However, nearly all of the differences in ΔSOA/ΔCO come prior to the first transect, meaning it is difficult to tell which SOA_{Pre} scenario agrees best with observations. The SOA fraction at 4 hr is around 15% in the higher emissions scenario and around 8% in the lower (Figure S5 in Supporting Information S1). The rapid formation of SOA in fresh smoke (<1 h) has been noted in prior studies (e.g., Akherati et al., 2022; Bian et al., 2017), and the lack of observations in this range has been noted as a potential explanation for discrepancies in OA evolution between lab and field studies. Our study supports these prior claims. The OPOA Off simulation has the lowest amount of Δ(POA + OPOA)/ΔCO as it only represents evaporated POA. As the fragmentation fraction (F) decreases, the Δ(POA + OPOA)/ΔCO is higher throughout the simulation due to the oxidation reaction of the POA volatility bins yielding a higher fraction in lower volatility bins, which favors the aerosol phase leading to less of a net decrease in ΔOA/ΔCO. The impact of the fragmentation fraction on observation agreement is minor through the first four transects, where all simulations have ΔOA/ΔCO within the error bars of the observations (Figure S4e in Supporting Information S1). At the last transect, the simulations with less fragmentation (more functionalization) have ΔOA/ΔCO slightly above the uncertainty of the observations; however, the observed ΔOA/ΔCO at the final transect does not seem consistent with the trend of the prior transects. The OPOA fraction increases ranging from around 5% up to 15%. The fraction of POA remaining at 4 hr in the highest fragmentation cases is high compared to that suggested by recent studies, whereas the fraction of POA remaining in simulations with fragmentation less than or equal to 0.25 is comparable to recent studies (Akherati et al., 2020, 2022). There are some impacts on the D_{pm} as the scenarios with more evaporation tend to have smaller particles. However, the impact of the OA aging sensitivity simulations on D_{pm} (Figure S4 in Supporting Information S1) is smaller than the near aircraft altitude impact on D_{pm} (Figure 2).

We are focused on the evolution of aerosols in the smoke plume; however, the model does capture some of the observed evolution of O_3, NO_X, and j_{HONO} prior to 2 hr of aging (Figure S6 in Supporting Information S1). Additionally, the OH concentrations in the model are consistent with Wang et al. (2021) and Liao et al. (2021). After 2 hr of aging, there are discrepancies in the trend in j_{HONO} as a result of the sun setting in the model, but due to the non-Lagrangian sampling, the sun has not set at that smoke age in the observations. This effect of the solar zenith angle is also seen in the decrease in OH (Figure 2d). Gas-phase evolution in this wildfire plume was the focus of the Wang et al. (2021) study; at the aircraft altitude, the results of our study are similar in the near-term aging, suggesting that the new coupling of TUV in our simulations is working as expected.

3.2. Simulated Vertical and Horizontal Variability in In-Plume Evolution

As discussed for the DIAL-HSRL comparisons, both the simulated plume and the observed plume have a concentrated portion in the FT with a less concentrated portion that mixes down to the surface (Figure 1). There are no measurements at altitudes other than the aircraft altitude, besides the DIAL-HSRL, available for this smoke plume. The ability of the model to represent the DIAL-HSRL measurements and the aerosol evolution at aircraft level (as was discussed in Section 3.1) leads us to believe there is credibility to the model in both the FT (where the aircraft sampled) and in the PBL. In Section 4, we discuss suggestions for future field campaigns to improve the vertical sampling of smoke plumes. According to the model, at 0 hr of aging, the total ΔCO burden in the FT and the PBL are roughly equal at 0 hr of aging with a slight increase in the PBL fraction as the plume ages due to dilution differences and entrainment between the FT and PBL (Figure 3). Due to the equal amounts of smoke present in the FT and PBL, we make comparisons between the evolution of the PBL and FT portions of the plume and discuss implications of the horizontal and vertical structure on the modeled evolution.

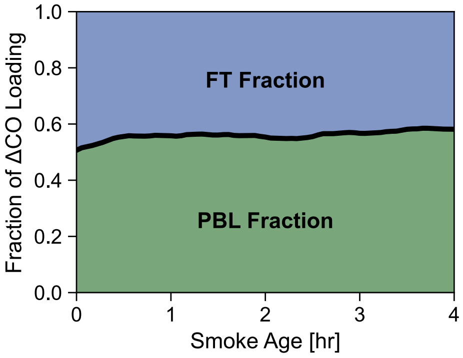

Figure 3. The fraction of total ΔCO loading in the free troposphere (blue) and in the PBL (green) as a function of smoke age. The ΔCO loading is defined in Equation 1.

The ΔCO structure in the plume (Figure 4a) illustrates the concentration gradients between the FT and PBL portions of the plume. At 0 hr of aging, the plume is not yet well mixed in the PBL with concentrations generally being lowest (ΔCO < 1,000 ppbv) near the surface and increasing with height until peaking around 2,100 m AGL at a ΔCO of around 8,000 ppbv (Figure S7a in Supporting Information S1). By 0.8 hr, the ΔCO in the PBL is well-mixed vertically with horizontally average concentrations around 1,100 ppbv throughout, whereas horizontally average concentrations in the FT are above 6,000 ppbv. From 0.8 hr aging (first observation transect) to 3.2 hr aging (last observation transect), the in-plume ΔCO mean in the PBL decreases from 1,000 to 720 ppbv while the FT in-plume mean decreases from 8,000 to 3,000 ppbv in the FT. Additionally, near the top of the PBL ΔCO tends to be greater than near the surface of the PBL due to entrainment from the more concentrated PBL into the FT. There is also movement from the PBL into the FT as shown by the top left side of the plume increasing in altitude from 0.8 to 2.0 hr. In terms of horizontal variability, the FT plume generally has larger variations in ΔCO than the PBL plume. Overall, after the initial fast dilution vertically in the PBL (creating the lower overall mixing ratios), the subsequent dilution tends to be slower in the PBL than in the FT.

Coagulation is faster in the FT than in the less concentrated PBL portion (Figures 4e–4l). At the time of the last transect (3.2 hr aging), this vertical gradient in coagulation results in a D_{pm} of 300 nm in the most concentrated portion of the FT and 200 nm at the surface, meaning aerosol diameter increased more in the FT than the PBL relative to the initial diameter of 110 nm. ΔN/ΔCO is initially around 125 scm^{-3} $ppbv^{-1}$ throughout all altitudes

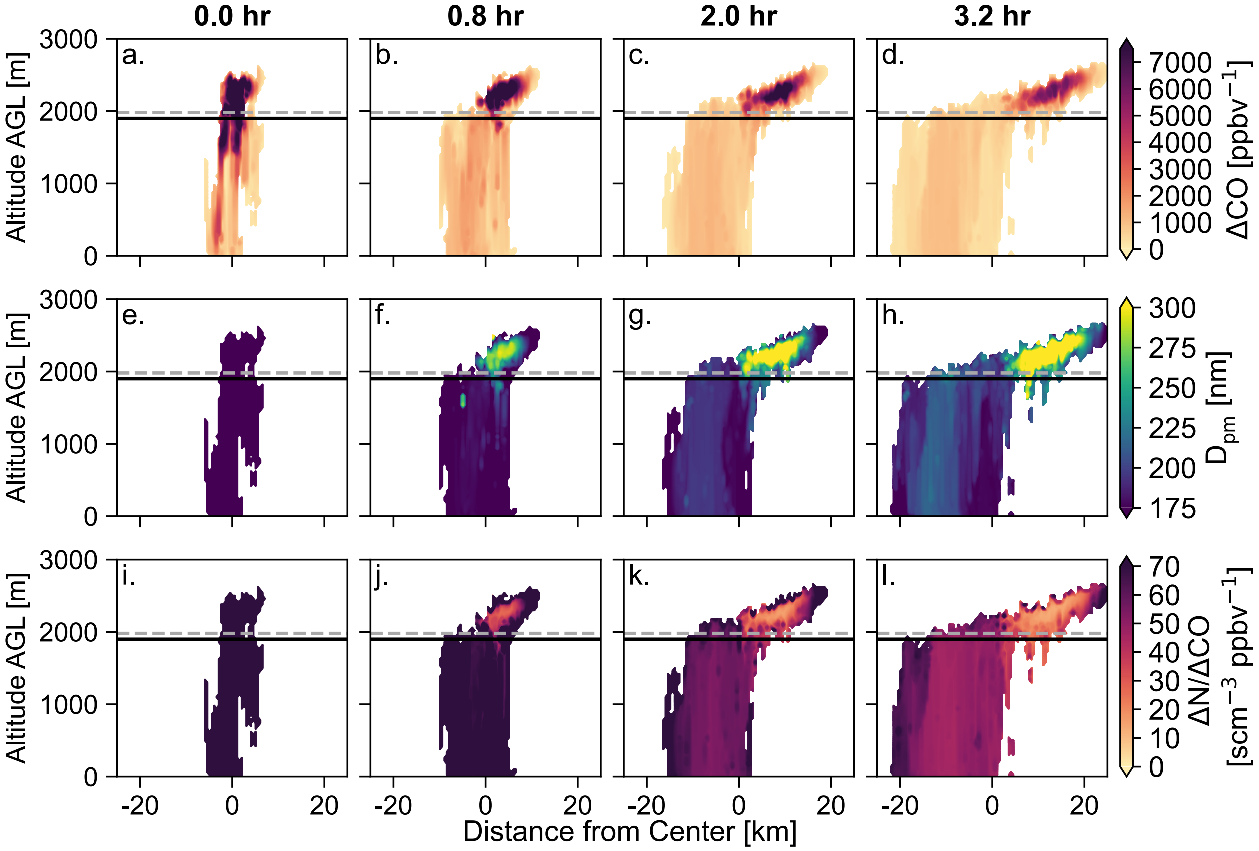

Figure 4. (a)–(d) ΔCO, (e)–(h) modeled D_{pm}, (i)–(l) modeled ΔN/ΔCO as a function of distance from center and altitude above ground level at four smoke ages downwind. The solid black horizontal line is the height of the PBL. The dashed gray line is the height of the aircraft that sampled the plume. Plume-average vertical profiles of these quantities are located in Figure S7 in Supporting Information S1.

of the plume. At 3.2 hr of aging, the faster coagulation in the FT has decreased the ΔN/ΔCO to 15 $\mathrm{scm^{-3}\ ppbv^{-1}}$, whereas the ΔN/ΔCO in the PBL is approximately 50 $\mathrm{scm^{-3}\ ppbv^{-1}}$. An important limitation of our study is the lack of ground observations with size distribution measurements in this size range; we believe that future field campaigns should plan to take measurements at multiple altitudes at similar times to better understand the vertical gradients in plumes. At the aircraft altitude, we can understand some of the horizontal gradients in the diameter. At 0.8 hr, there is a 10 nm difference between D_{pm} at the edge of the plume (215 nm) and the core of the plume (225 nm) for the model and the observations. At 3.2 hr of aging, the observed difference in D_{pm} between the edge (245 nm) and core (280 nm) of the plume was about 35 nm (June et al., 2022), whereas the model has 40 nm difference between the edge (240 nm) and core (280 nm) of the plume at the same time. These results confirm that the mixing throughout the plume influences particle size on the dilute edges of the plume, as the SAM-ASP-TUV simulation more closely represents the gradients in D_{pm} growth than a box model simulation, which assumes no mixing (June et al., 2022). Although coagulation dominates the changes in D_{pm}, there are also effects on the D_{pm} due to gradients in ΔOA/ΔCO, which will be discussed below.

Figure 5 shows the cross sections through the plume at four smoke ages of OA-relevant properties. ΔOA/ΔCO (Figures 5a–5d) shows slight net OA condensation in the PBL and net OA evaporation in the FT with horizontal gradients at each altitude. At 0.8 hr of aging, the more concentrated parts of the plume at each altitude horizontally tend to have higher ΔOA/ΔCO. Prior studies have also tended to see that at the time of the first transect, the most concentrated plumes or parts of the plume have higher ΔOA/ΔCO (Akherati et al., 2022; Bian et al., 2017; Hodshire et al., 2021; Hodshire, Akherati, et al., 2019; June et al., 2022; Peng et al., 2020). Vertically at 0.8 hr of aging, the ΔOA/ΔCO increases from 0.49 $\mu\mathrm{g\ sm^{-3}\ ppbv^{-1}}$ at the surface to 0.62 $\mu\mathrm{g\ sm^{-3}\ ppbv^{-1}}$ at the PBL top, whereas the ΔOA/ΔCO in the FT is around 0.70 ± 0.06 $\mu\mathrm{g\ sm^{-3}\ ppbv^{-1}}$. By 3.2 hr of aging, the ΔOA/ΔCO in the PBL ranges from 0.51 $\mu\mathrm{g\ sm^{-3}\ ppbv^{-1}}$ at the surface to 0.60 $\mu\mathrm{g\ sm^{-3}\ ppbv^{-1}}$ at the PBL top. In the FT at 3.2 hr of aging, the ΔOA/ΔCO has decreased by around 0.05 $\mu\mathrm{g\ sm^{-3}\ ppbv^{-1}}$ except for near the top of the plume, which experienced close to a net-zero change. The differences in the ΔOA/ΔCO evolution between the PBL and the FT can be explained using differences in dilution, concentration, temperature, and oxidation throughout the plume.

At all altitudes, dilution is contributing to the evaporation of POA (Figures 5e–5h). Initially, all of the OA mass is POA, at 0.8 hr of aging the POA fraction is 0.86 at the surface, 0.88 at the PBL top, and 0.91 in the FT. Then, at 3.2 hr of aging, the POA fraction is 0.76 at the surface, 0.78 at the PBL top, and 0.84 in the FT. At 0.0 hr aging, due to faster dilution in the PBL than the FT during emissions, there is a lower ΔPOA/ΔCO ratio in the PBL than in the FT (Figure S8 in Supporting Information S1) explaining the lower initial ΔOA/ΔCO in the PBL. After emissions are complete (and chemistry turns on), slower dilution in the PBL favors slower evaporation of POA in the PBL than in the FT. However, the vertical temperature gradient is also influential in the POA evaporation in the plume. At the surface, the temperature is 300 K, whereas at the PBL top, the temperature is 280 K. Temperatures in the FT plume range from 280 to 278 K (Figure S7e in Supporting Information S1). Within the PBL, where dilution is fairly constant with height, the lower remaining POA fraction at the surface than at the PBL top is explained by the warmer temperature at the surface. The warmer temperature favors more organic matter partitioning to vapors at the surface. In the FT, the temperature is lower than in the PBL, but dilution (after the initial fast PBL dilution) is faster, which leads to steady POA evaporation in the FT throughout the simulation. The temperature effect on ΔOA/ΔCO suggested by our modeling work is consistent with an observational study that showed ground measurements having an OA normalized excess mixing ratio that was two-thirds of that measured at aircraft altitudes with this effect being shown for samplings of wildfire smoke and agriculture smoke in multiple field campaigns in the United States (Pagonis et al., 2023). This study also showed substantial evaporation for descending smoke and in an onboard thermal denuder with ∼30 K of heating (Pagonis et al., 2023). Additionally, the temperature effect contributing to more evaporation at the surface than at the top of the PBL affects D_{pm}. At each age, the D_{pm} is around 5%–10% smaller at the surface than at the top of the PBL.

Differences in chemistry within the plume explain the remaining FT/PBL differences in the ΔOA/ΔCO evolution and help to explain the horizontal variability throughout the plume. In the PBL, the OPOA fraction ranges from 0.09 to 0.06 at 0.8 hr and 0.16 to 0.14 at 3.2 hr. In the FT, the OPOA fraction is 0.005 and 0.08 at 0.8 and 3.2 hr, respectively (Figures 5i–5l). The SOA fraction in the PBL is 0.05 at 0.8 hr of aging and 0.06 at 3.2 hr. In the FT, the SOA fraction is 0.09 and 0.08 at 0.8 and 3.2 hr, respectively (Figures 5m–5p). In terms of absolute enhancement ratios, the FT tends to have higher ΔSOA/ΔCO at all ages than the PBL, whereas the PBL tends to have a higher ΔOPOA/ΔCO than the FT due to POA evaporation driving OPOA formation in the PBL (Figure S8 in Supporting Information S1). Prior to the first transect, the SOA formation is faster in the FT than in the PBL due

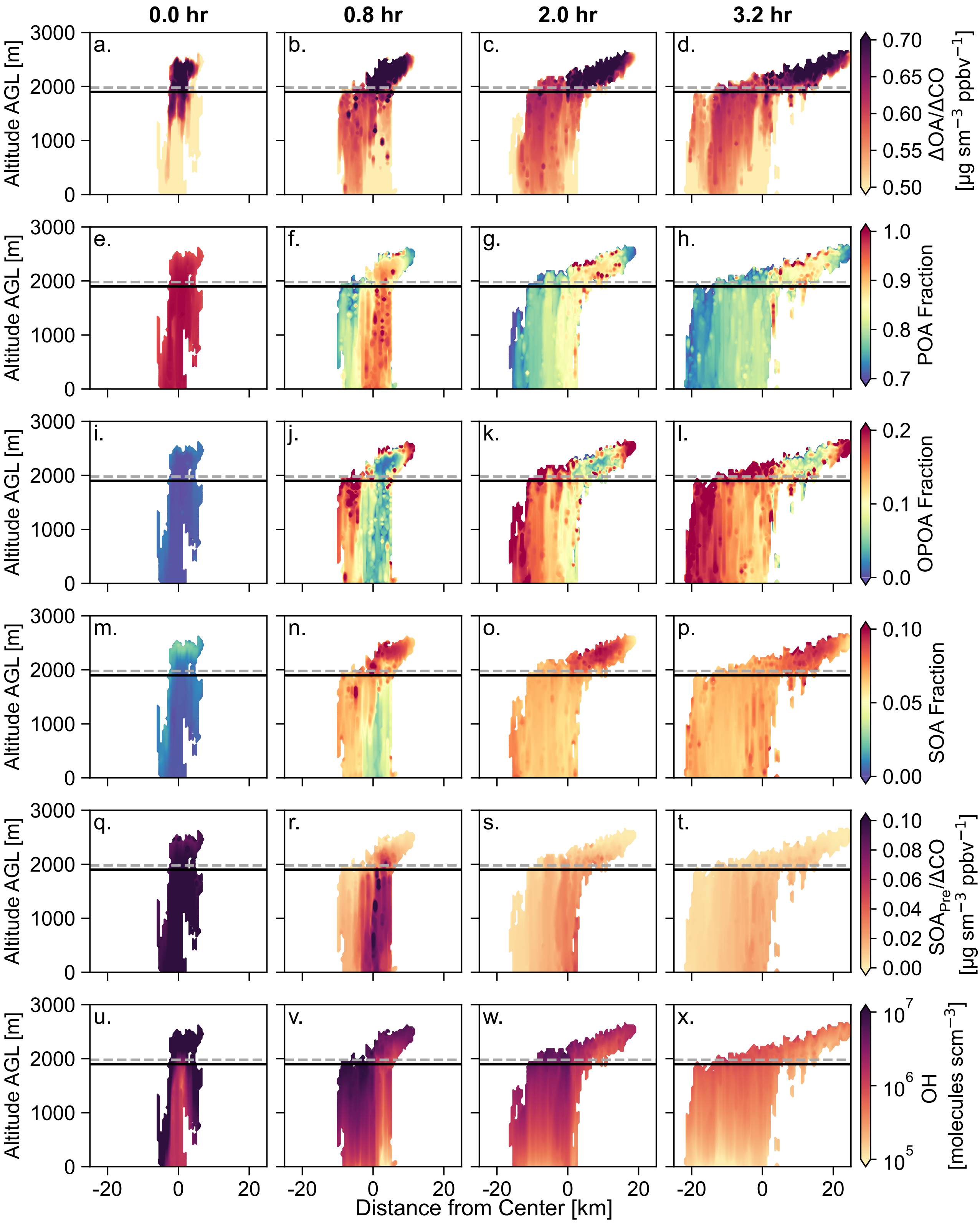
0.0 hr
0.8 hr
2.0 hr
3.2 hr
a.
b.
c.
d.
e.
f.
g.
h.
i.
j.
k.
l.
m.
n.
o.
p.
q.
r.
s.
t.
u.
v.
w.
x.
Altitude AGL [m]
3000
2000
1000
0
0.70
0.65
0.60
0.55
0.50
ΔOA/ΔCO [μg sm⁻³ ppbv⁻¹]
1.0
0.9
0.8
0.7
POA Fraction
0.2
0.1
0.0
OPOA Fraction
0.10
0.05
0.00
SOA Fraction
0.10
0.08
0.06
0.04
0.02
0.00
SOA_Pre/ΔCO [μg sm⁻³ ppbv⁻¹]
10^7
10^6
10^5
OH [molecules scm⁻³]
-20
0
20
Distance from Center [km]

Figure 5.

to having more SOA precursors (Figures 5q–5t). After the first transect, SOA formation slows in the FT (no more SOA precursor), whereas some SOA precursor remains in the PBL allowing for some additional SOA formation there. However, SOA and OPOA formation in the PBL is impacted by the concentrated FT plume above resulting in lower OH concentrations in parts of the PBL (Figures 5u–5x).

Impacts of OH are also seen in the horizontal gradients of OPOA and SOA at each altitude. OH suppression in much of the plume is driven by attenuation of solar radiation, whereas OH enhancement in dilute parts of the plume results from rapid HONO photolysis being the dominant source of OH in wildfire plumes (Wang et al., 2021). In dilute, sunnier portions of the plume (highest OH concentrations), the OPOA fraction exceeds 20% by the end of the simulation. But in darker parts of the plume (lowest OH), such as the concentrated levels of the FT and the right side of the PBL plume, OPOA formation is slow, with the fraction of OA that is OPOA never exceeding 7% in parts of the FT and just reaching 10% in parts of the PBL. For SOA, the sunnier portions of the PBL have lower concentrations of SOA precursor than the FT and the non-sunny parts of the PBL limiting the SOA formation. The gradients in light in the plume are evident in the horizontal and vertical gradients of $\Delta O_3/\Delta CO$ and j_{HONO}, where regions of high OH tend to have faster photolysis and faster O_3 formation (Figure S9 in Supporting Information S1). In addition to photolysis gradients due to the concentration of the plume, the plume was oriented west-east, resulting in gradients in photolysis due to the position of the sun. Overall, the concentration and temperature gradients result in a higher SOA fraction in the FT due to the colder temperatures and higher SOA_{Pre} and a higher OPOA fraction in the PBL due to more POA evaporation as a result of warmer temperatures. The assumed volatility distribution of POA/OPOA and SOA likely influences these results (May et al., 2015; Pagonis et al., 2023); however, the volatility distribution assumed in our study is consistent with prior studies (Jen et al., 2019; May et al., 2013; Shrivastava et al., 2024) and results are in agreement with the observed ΔOA/ΔCO at aircraft altitude.

4. Conclusions, Implications, and Future Work

In this study, we evaluate the SAM-ASP model coupled with TUV at the aircraft altitude and examine differences in free tropospheric and PBL evolution seen in the Williams Flats Fire sampled by the FIREX-AQ field campaign on 3 August 2019. At the aircraft altitude, the model explains the observed dilution, coagulation, and net OA evaporation. After 4 hr of aging, the ΔOA/ΔCO at the aircraft altitude is 15% OPOA, 6% SOA, and 79% POA; however, nearly all of the SOA formation occurred prior to the first transect (45 min downwind). Vertically, in agreement with DIAL-HSRL lidar observations, a significant portion of the plume was present in the FT and PBL with near equal distribution between the FT and PBL in the model. Generally, there was a lower ΔOA/ΔCO in the PBL as a result of warmer temperatures. Additionally, the lower concentrations throughout the simulation in the PBL lead to slower coagulation. Shading of the PBL due to the concentrated plume above lowers the OH concentration of non-sunny parts of the PBL slowing the SOA formation there.

There are several implications and needs for future work as a result of the differences in smoke plume evolution between the PBL and FT. The first is coarse global and regional models cannot capture these plume-scale effects even with current parameterizations. One such parameterization is a parameterization for biomass burning coagulation (Sakamoto et al., 2016). This parameterization can be used in coarse resolution models to increase the size of emitted biomass burning aerosols due to the effects of coagulation (Ramnarine et al., 2019). However, this parameterization calculates one growth rate for a plume. The Sakamoto et al. (2016) parameterization would not capture the faster coagulation in the FT and the slower coagulation in the PBL seen in our study. Additionally, this specific parameterization does not include effects of OA evaporation/condensation on particle size, so it would not capture the evaporation driven size differences within the PBL. Future versions of parameterizations should include considerations of variability of aging within a plume. For coagulation, this would mean having higher coagulation rates in the core of the plume with slower rates on the edges or in faster diluting regions (e.g., PBL).

Figure 5. Modeled (a)–(d) ΔOA/ΔCO, (e)–(h) primary organic aerosol (POA) fraction, (i)–(l) oxidized primary organic aerosol (OPOA) fraction, (m)–(p) secondary organic aerosol (SOA) fraction, (q)–(t) SOA pre/ΔCO, and (u)–(x) OH as a function of distance from center and height at four times downwind. The solid black horizontal line is the height of the PBL. The dashed gray line is the height of the aircraft that sampled the plume. Plume-average vertical profiles of these quantities are located in Figure S7 in Supporting Information S1. The enhancement ratios for POA, OPOA, and SOA (rather than fractions) are shown in Figure S8 in Supporting Information S1.

For subgrid plume processing of OA, we suggest having a temperature dependent parameterization for POA evolution and consideration of vertical gradients in OH for SOA/OPOA formation.

The second implication is effects on air quality due to the temperature driven evaporation of OA near the surface. Since typically, there are higher temperatures at the surface than aloft, this would tend to increase the amount of reactive organic carbon in the gas phase rather than in the particulate phase. Pagonis et al. (2023) showed that including observationally constrained volatility information in a one-day simulation using High Resolution Rapid Refresh Smoke (HRRR-Smoke) model reduced surface smoke concentrations by 30%.

Overall, these implications suggest the need for more precise plume injection heights (including multiple potential detrainment levels for the same fire) in models as the aging of the plume will be different at different levels. Even if better parameterizations for these subgrid processes such as coagulation, rapid early production, and evaporation are developed, accurately representing plumes in global and regional models requires accurate plume injection heights at multiple potential detrainment levels. The GFAS biomass burning emissions inventory includes estimates of plume injection height (Rémy et al., 2017); however, it includes one estimate per day and may be biased low (Walter et al., 2016), and it does not include multiple peak levels of detrainment. Plume rise models coupled with atmospheric models may allow for better representation of plume dynamics (Walter et al., 2016) but at a higher computational expense, which is likely already increased due to the added parameterizations needed to represent the OA evaporation/condensation and coagulation processes. Therefore, continued work on improving plume injection height in emission inventories and simulations is needed (Cheeseman et al., 2020; X. Chen et al., 2021; Lyapustin et al., 2020).

Finally, to develop the parameterizations that would be needed to represent the differences between FT and PBL smoke plume evolution, additional observational evidence is needed to support the simulated impacts shown in this study and to reduce the limitations induced by the observational uncertainty. At the altitude sampled by the aircraft, our model-observation comparisons are limited in that our model is a Lagrangian model moving with the mean wind speed of the plume injection, whereas the airplane moved more than two-times faster than this wind speed. Therefore, it is difficult to discern if biases are the result of model biases in emissions or processes, or if it is the result of the observations being influenced by changing fire and environmental conditions. Additionally, we were unable to evaluate the particle size and OA evolution at heights other than the single aircraft altitude located in the FT. From these limitations, we suggest future field campaigns work to remedy these limitations through changes to sampling design through increased use of sampling designs like those used with the Twin Otter aircraft during FIREX-AQ or those used during the California Fire Dynamics Experiment (Carroll et al., 2024; Washenfelder et al., 2022). For example, we recommend having a mobile laboratory with the same instrumentation as the aircraft, and when possible, sample the same fires as the aircraft. Future campaigns should continue to work toward lowering the age of the first transect downind. The first transect used in this study was nearly an hour downwind, sampling late in the plume limits the ability to use OA factors from the AMS to look at the early SOA formation. We also recommend having the aircraft sample at multiple heights (when allowed) at every transect downwind (perhaps lowering the age of the oldest smoke sampled to keep the same flight time), which would decrease the speed that the aircraft moves downwind, moving closer to Lagrangian sampling, while also improving the quantity of vertical measurements.

Acknowledgments

This work is supported by the US NOAA, an Office of Science, Office of Atmospheric Chemistry, Carbon Cycle, and Climate program under the cooperative agreement award NA21OAR4310128; and the US NSF Atmospheric Chemistry program under Grants AGS-1950327 and AGS-2211153. This publication was partly developed under Assistance Agreement no. R840008 awarded by the U.S. Environmental Protection Agency to Colorado State University. It has not been formally reviewed by EPA. The views expressed in this document are solely those of the authors and do not necessarily reflect those of the Agency. EPA does not endorse any products or commercial services mentioned in this publication. HG, DJP, PCJ, and JLJ acknowledge support from NASA, Grants 80NSSC21K1451 and 80NSSC23K0828. We thank Jonathan Hair and Marta Fenn for their work in taking the DIAL-HSRL measurements. We thank the pilots and crew of the NASA DC-8 and the FIREX-AQ project scientists: Jim Crawford, Jack Dibb, Carsten Warneke, Shuka Schwarz, and Barry Lefer.

Data Availability Statement

All observation data used in this study are publicly available in the NASA FIREX-AQ data archive (FIREX-AQ science team, 2019). Version 1.0.0 of SAM-ASP-TUV used in this study as well as the input files are publicly available (June & Alvarado, 2024).

References

Adachi, K., Dibb, J. E., Scheuer, E., Katich, J. M., Schwarz, J. P., Perring, A. E., et al. (2022). Fine ash-bearing particles as a major aerosol component in biomass burning smoke. *Journal of Geophysical Research: Atmospheres*, *127*(2), e2021JD035657. https://doi.org/10.1029/2021JD035657

Ahmadov, R., McKeen, S. A., Robinson, A. L., Bahreini, R., Middlebrook, A. M., de Gouw, J. A., et al. (2012). A volatility basis set model for summertime secondary organic aerosols over the eastern United States in 2006. *Journal of Geophysical Research*, *117*, D06301. https://doi.org/10.1029/2011jd016831

Akagi, S. K., Craven, J. S., Taylor, J. W., McMeeking, G. R., Yokelson, R. J., Burling, I. R., et al. (2012). Evolution of trace gases and particles emitted by a chaparral fire in California. *Atmospheric Chemistry and Physics*, *12*(3), 1397–1421. https://doi.org/10.5194/acp-12-1397-2012

Akagi, S. K., Yokelson, R. J., Wiedinmyer, C., Alvarado, M. J., Reid, J. S., Karl, T., et al. (2011). Emission factors for open and domestic biomass burning for use in atmospheric models. *Atmospheric Chemistry and Physics*, *11*(9), 4039–4072. https://doi.org/10.5194/acp-11-4039-2011

Akherati, A., He, Y., Coggon, M. M., Koss, A. R., Hodshire, A. L., Sekimoto, K., et al. (2020). Oxygenated aromatic compounds are important precursors of secondary organic aerosol in biomass-burning emissions. *Environmental Science and Technology*, *54*(14), 8568–8579. https://doi.org/10.1021/acs.est.0c01345

Akherati, A., He, Y., Hu, L., Fischer, E. V., Jen, C. N., Goldstein, A. H., et al. (2022). Dilution and photooxidation driven processes explain the evolution of organic aerosol in wildfire plumes. *Environmental Science: Atmospheres*, *2*(5), 1000–1022. https://doi.org/10.1039/D1EA00082A

Alvarado, M. J., Lonsdale, C. R., Macintyre, H. L., Bian, H., Chin, M., Ridley, D. A., et al. (2016). Evaluating model parameterizations of submicron aerosol scattering and absorption with in situ data from ARCTAS 2008. *Atmospheric Chemistry and Physics*, *16*(14), 9435–9455. https://doi.org/10.5194/acp-16-9435-2016

Alvarado, M. J., Lonsdale, C. R., Yokelson, R. J., Akagi, S. K., Coe, H., Craven, J. S., et al. (2015). Investigating the links between ozone and organic aerosol chemistry in a biomass burning plume from a prescribed fire in California chaparral. *Atmospheric Chemistry and Physics*, *15*(12), 6667–6688. https://doi.org/10.5194/acp-15-6667-2015

Alvarado, M. J., & Prinn, R. G. (2009). Formation of ozone and growth of aerosols in young smoke plumes from biomass burning: 1. Lagrangian parcel studies. *Journal of Geophysical Research*, *114*(D9), D09306. https://doi.org/10.1029/2008JD011144

Andreae, M. O. (2019). Emission of trace gases and aerosols from biomass burning – An updated assessment. *Atmospheric Chemistry and Physics*, *19*(13), 8523–8546. https://doi.org/10.5194/acp-19-8523-2019

Andreae, M. O., & Merlet, P. (2001). Emission of trace gases and aerosols from biomass burning. *Global Biogeochemical Cycles*, *15*(4), 955–966. https://doi.org/10.1029/2000GB001382

Bahreini, R., Ervens, B., Middlebrook, A. M., Warneke, C., de Gouw, J. A., DeCarlo, P. F., et al. (2009). Organic aerosol formation in urban and industrial plumes near houston and dallas, texas. *Journal of Geophysical Research*, *114*(D7), D00F16. https://doi.org/10.1029/2008JD011493

Bahreini, R., Keywood, M. D., Ng, N. L., Varutbangkul, V., Gao, S., Flagan, R. C., et al. (2005). Measurements of secondary organic aerosol from oxidation of cycloalkenes, terpenes, and m-xylene using an aerodyne aerosol mass spectrometer. *Environmental Science and Technology*, *39*(15), 5674–5688. https://doi.org/10.1021/es048061a

Bais, A. F., Madronich, S., Crawford, J., Hall, S. R., Mayer, B., van Weele, M., et al. (2003). International photolysis frequency measurement and model intercomparison (IPMMI): Spectral actinic solar flux measurements and modeling. *Journal of Geophysical Research*, *108*(D16), 8612. https://doi.org/10.1029/2002JD002891

Bian, Q., Jathar, S. H., Kodros, J. K., Barsanti, K. C., Hatch, L. E., May, A. A., et al. (2017). Secondary organic aerosol formation in biomass-burning plumes: Theoretical analysis of lab studies and ambient plumes. *Atmospheric Chemistry and Physics*, *17*(8), 5459–5475. https://doi.org/10.5194/acp-17-5459-2017

Bilsback, K. R., He, Y., Cappa, C. D., Chang, R. Y.-W., Croft, B., Martin, R. V., et al. (2023). Vapors are lost to walls, not to particles on the wall: Artifact-corrected parameters from chamber experiments and implications for global secondary organic aerosol. *Environmental Science and Technology*, *57*(1), 53–63. https://doi.org/10.1021/acs.est.2c03967

Bohren, C. F., & Huffman, D. R. (2008). *Absorption and scattering of light by small particles*. John Wiley and Sons.

Bond, T. C., Doherty, S. J., Fahey, D. W., Forster, P. M., Berntsen, T., DeAngelo, B. J., et al. (2013). Bounding the role of black carbon in the climate system: A scientific assessment. *Journal of Geophysical Research: Atmospheres*, *118*(11), 5380–5552. https://doi.org/10.1002/jgrd.50171

Bourgeois, I., Peischl, J., Neuman, J. A., Brown, S. S., Allen, H. M., Campuzano-Jost, P., et al. (2022). Comparison of airborne measurements of NO, NO_2, HONO, NO_y, and CO during FIREX-AQ. *Atmospheric Measurement Techniques*, *15*(16), 4901–4930. https://doi.org/10.5194/amt-15-4901-2022

Capes, G., Johnson, B., McFiggans, G., Williams, P. I., Haywood, J., & Coe, H. (2008). Aging of biomass burning aerosols over West Africa: Aircraft measurements of chemical composition, microphysical properties, and emission ratios. *Journal of Geophysical Research*, *113*(D23), D00C15. https://doi.org/10.1029/2008JD009845

Carrico, C. M., Petters, M. D., Kreidenweis, S. M., Collett, J. L., Jr., Engling, G., & Malm, W. C. (2008). Aerosol hygroscopicity and cloud droplet activation of extracts of filters from biomass burning experiments. *Journal of Geophysical Research*, *113*(D8), D08206. https://doi.org/10.1029/2007JD009274

Carroll, B. J., Brewer, W. A., Strobach, E., Lareau, N., Brown, S. S., Valero, M. M., et al. (2024). Measuring Coupled Fire–Atmosphere Dynamics: The California Fire Dynamics Experiment (CalFiDE). https://doi.org/10.1175/BAMS-D-23-0012.1

Charan, S. M., Huang, Y., & Seinfeld, J. H. (2019). Computational simulation of secondary organic aerosol formation in laboratory chambers. *Chemical Reviews*, *119*(23), 11912–11944. https://doi.org/10.1021/acs.chemrev.9b00358

Cheeseman, M., Ford, B., Volckens, J., Lyapustin, A., & Pierce, J. R. (2020). The relationship between MAIAC smoke plume heights and surface PM. *Geophysical Research Letters*, *47*(17), e2020GL088949. https://doi.org/10.1029/2020GL088949

Chen, J., Li, C., Ristovski, Z., Milic, A., Gu, Y., Islam, M. S., et al. (2017). A review of biomass burning: Emissions and impacts on air quality, health and climate in China. *Science of The Total Environment*, *579*, 1000–1034. https://doi.org/10.1016/j.scitotenv.2016.11.025

Chen, X., Wang, J., Xu, X., Zhou, M., Zhang, H., Castro Garcia, L., et al. (2021). First retrieval of absorbing aerosol height over dark target using TROPOMI oxygen B band: Algorithm development and application for surface particulate matter estimates. *Remote Sensing of Environment*, *265*, 112674. https://doi.org/10.1016/j.rse.2021.112674

Cubison, M. J., Ortega, A. M., Hayes, P. L., Farmer, D. K., Day, D., Lechner, M. J., et al. (2011). Effects of aging on organic aerosol from open biomass burning smoke in aircraft and laboratory studies. *Atmospheric Chemistry and Physics*, *11*(23), 12049–12064. https://doi.org/10.5194/acp-11-12049-2011

Decker, Z. C. J., Wang, S., Bourgeois, I., Campuzano Jost, P., Coggon, M. M., DiGangi, J. P., et al. (2021). Novel analysis to quantify plume crosswind heterogeneity applied to biomass burning smoke. *Environmental Science and Technology*, *55*(23), 15646–15657. https://doi.org/10.1021/acs.est.1c03803

Dzepina, K., Volkamer, R. M., Madronich, S., Tulet, P., Ulbrich, I. M., Zhang, Q., et al. (2009). Evaluation of recently-proposed secondary organic aerosol models for a case study in Mexico City. *Atmospheric Chemistry and Physics*, *9*(15), 5681–5709. https://doi.org/10.5194/acp-9-5681-2009

FIREX-AQ science team. (2019). Fire influence on regional to global environments and air quality [Dataset]. *NASA*. https://doi.org/10.5067/SUBORBITAL/FIREXAQ2019/DATA001

Ford, B., Val Martin, M., Zelasky, S. E., Fischer, E. V., Anenberg, S. C., Heald, C. L., & Pierce, J. R. (2018). Future fire impacts on smoke concentrations, visibility, and health in the contiguous United States. *GeoHealth*, *2*(8), 229–247. https://doi.org/10.1029/2018GH000144

Garofalo, L. A., Pothier, M. A., Levin, E. J. T., Campos, T., Kreidenweis, S. M., & Farmer, D. K. (2019). Emission and evolution of submicron organic aerosol in smoke from wildfires in the western United States. *ACS Earth and Space Chemistry*, *3*(7), 1237–1247. https://doi.org/10.1021/acsearthspacechem.9b00125

Gkatzelis, G. I., Coggon, M. M., Stockwell, C. E., Hornbrook, R. S., Allen, H., Apel, E. C., et al. (2024). Parameterizations of US wildfire and prescribed fire emission ratios and emission factors based on FIREX-AQ aircraft measurements. *Atmospheric Chemistry and Physics*, *24*(2), 929–956. https://doi.org/10.5194/acp-24-929-2024

Granier, C., Bessagnet, B., Bond, T., D'Angiola, A., Denier van der Gon, H., Frost, G. J., et al. (2011). Evolution of anthropogenic and biomass burning emissions of air pollutants at global and regional scales during the 1980–2010 period. *Climatic Change*, *109*(1), 163–190. https://doi.org/10.1007/s10584-011-0154-1

Grieshop, A. P., Logue, J. M., Donahue, N. M., & Robinson, A. L. (2009). Laboratory investigation of photochemical oxidation of organic aerosol from wood fires 1: Measurement and simulation of organic aerosol evolution. *Atmospheric Chemistry and Physics*, *9*(4), 1263–1277. https://doi.org/10.5194/acp-9-1263-2009

Guo, H., Campuzano-Jost, P., Nault, B. A., Day, D. A., Schroder, J. C., Kim, D., et al. (2021). The importance of size ranges in aerosol instrument intercomparisons: A case study for the atmospheric tomography mission. *Atmospheric Measurement Techniques*, *14*(5), 3631–3655. https://doi.org/10.5194/amt-14-3631-2021

Hatch, L. E., Luo, W., Pankow, J. F., Yokelson, R. J., Stockwell, C. E., & Barsanti, K. C. (2015). Identification and quantification of gaseous organic compounds emitted from biomass burning using two-dimensional gas chromatography–time-of-flight mass spectrometry. *Atmospheric Chemistry and Physics*, *15*(4), 1865–1899. https://doi.org/10.5194/acp-15-1865-2015

Hatch, L. E., Rivas-Ubach, A., Jen, C. N., Lipton, M., Goldstein, A. H., & Barsanti, K. C. (2018). Measurements of I/SVOCs in biomass-burning smoke using solid-phase extraction disks and two-dimensional gas chromatography. *Atmospheric Chemistry and Physics*, *18*(24), 17801–17817. https://doi.org/10.5194/acp-18-17801-2018

Hatch, L. E., Yokelson, R. J., Stockwell, C. E., Veres, P. R., Simpson, I. J., Blake, D. R., et al. (2017). Multi-instrument comparison and compilation of non-methane organic gas emissions from biomass burning and implications for smoke-derived secondary organic aerosol precursors. *Atmospheric Chemistry and Physics*, *17*(2), 1471–1489. https://doi.org/10.5194/acp-17-1471-2017

Hecobian, A., Liu, Z., Hennigan, C. J., Huey, L. G., Jimenez, J. L., Cubison, M. J., et al. (2011). Comparison of chemical characteristics of 495 biomass burning plumes intercepted by the NASA DC-8 aircraft during the ARCTAS/CARB-2008 field campaign. *Atmospheric Chemistry and Physics*, *11*(24), 13325–13337. https://doi.org/10.5194/acp-11-13325-2011

Hennigan, C. J., Sullivan, A. P., Collett, J. L., Jr., & Robinson, A. L. (2010). Levoglucosan stability in biomass burning particles exposed to hydroxyl radicals. *Geophysical Research Letters*, *37*(9), L09806. https://doi.org/10.1029/2010GL043088

Hobbs, P. V., Reid, J. S., Kotchenruther, R. A., Ferek, R. J., & Weiss, R. (1997). Direct radiative forcing by smoke from biomass burning. *Science*, *275*(5307), 1777–1778. https://doi.org/10.1126/science.275.5307.1777

Hobbs, P. V., Sinha, P., Yokelson, R. J., Christian, T. J., Blake, D. R., Gao, S., et al. (2003). Evolution of gases and particles from a savanna fire in South Africa. *Journal of Geophysical Research*, *108*(D13), 8485. https://doi.org/10.1029/2002JD002352

Hodshire, A. L., Akherati, A., Alvarado, M. J., Brown-Steiner, B., Jathar, S. H., Jimenez, J. L., et al. (2019). Aging effects on biomass burning aerosol mass and composition: A critical review of field and laboratory studies. *Environmental Science and Technology*, *53*(17), 10007–10022. https://doi.org/10.1021/acs.est.9b02588

Hodshire, A. L., Bian, Q., Ramnarine, E., Lonsdale, C. R., Alvarado, M. J., Kreidenweis, S. M., et al. (2019). More than emissions and chemistry: Fire size, dilution, and background aerosol also greatly influence near-field biomass burning aerosol aging. *Journal of Geophysical Research: Atmospheres*, *124*(10), 5589–5611. https://doi.org/10.1029/2018JD029674

Hodshire, A. L., Ramnarine, E., Akherati, A., Alvarado, M. L., Farmer, D. K., Jathar, S. H., et al. (2021). Dilution impacts on smoke aging: Evidence in biomass burning observation project (BBOP) data. *Atmospheric Chemistry and Physics*, *21*(9), 6839–6855. https://doi.org/10.5194/acp-21-6839-2021

Huffman, J. A., Docherty, K. S., Aiken, A. C., Cubison, M. J., Ulbrich, I. M., DeCarlo, P. F., et al. (2009). Chemically-resolved aerosol volatility measurements from two megacity field studies. *Atmospheric Chemistry and Physics*, *9*(18), 7161–7182. https://doi.org/10.5194/acp-9-7161-2009

Janhäll, S., Andreae, M. O., & Pöschl, U. (2010). Biomass burning aerosol emissions from vegetation fires: Particle number and mass emission factors and size distributions. *Atmospheric Chemistry and Physics*, *10*(3), 1427–1439. https://doi.org/10.5194/acp-10-1427-2010

Jathar, S. H., Gordon, T. D., Hennigan, C. J., Pye, H. O. T., Pouliot, G., Adams, P. J., et al. (2014). Unspeciated organic emissions from combustion sources and their influence on the secondary organic aerosol budget in the United States. *Proceedings of the National Academy of Sciences*, *111*(29), 10473–10478. https://doi.org/10.1073/pnas.1323740111

Jen, C. N., Hatch, L. E., Selimovic, V., Yokelson, R. J., Weber, R., Fernandez, A. E., et al. (2019). Speciated and total emission factors of particulate organics from burning western US wildland fuels and their dependence on combustion efficiency. *Atmospheric Chemistry and Physics*, *19*(2), 1013–1026. https://doi.org/10.5194/acp-19-1013-2019

Jolleys, M. D., Coe, H., McFiggans, G., Taylor, J. W., O'Shea, S. J., Le Breton, M., et al. (2015). Properties and evolution of biomass burning organic aerosol from Canadian boreal forest fires. *Atmospheric Chemistry and Physics*, *15*(6), 3077–3095. https://doi.org/10.5194/acp-15-3077-2015

June, N. A., & Alvarado, M. (2024). SAM-ASP-TUV: v1.0.0 (v1.0.0) [Software]. *Zenodo*. https://doi.org/10.5281/zenodo.13385240

June, N. A., Hodshire, A. L., Wiggins, E. B., Winstead, E. L., Robinson, C. E., Thornhill, K. L., et al. (2022). Aerosol size distribution changes in FIREX-AQ biomass burning plumes: The impact of plume concentration on coagulation and OA condensation/evaporation. *Atmospheric Chemistry and Physics*, *22*(19), 12803–12825. https://doi.org/10.5194/acp-22-12803-2022

Kodros, J. K., Volckens, J., Jathar, S. H., & Pierce, J. R. (2018). Ambient particulate matter size distributions drive regional and global variability in particle deposition in the respiratory tract. *GeoHealth*, *2*(10), 298–312. https://doi.org/10.1029/2018GH000145

Koss, A. R., Sekimoto, K., Gilman, J. B., Selimovic, V., Coggon, M. M., Zarzana, K. J., et al. (2018). Non-methane organic gas emissions from biomass burning: Identification, quantification, and emission factors from PTR-ToF during the FIREX 2016 laboratory experiment. *Atmospheric Chemistry and Physics*, *18*(5), 3299–3319. https://doi.org/10.5194/acp-18-3299-2018

Lamarque, J.-F., Bond, T. C., Eyring, V., Granier, C., Heil, A., Klimont, Z., et al. (2010). Historical (1850–2000) gridded anthropogenic and biomass burning emissions of reactive gases and aerosols: Methodology and application. *Atmospheric Chemistry and Physics*, *10*(15), 7017–7039. https://doi.org/10.5194/acp-10-7017-2010

Lee, L. A., Pringle, K. J., Reddington, C. L., Mann, G. W., Stier, P., Spracklen, D. V., et al. (2013). The magnitude and causes of uncertainty in global model simulations of cloud condensation nuclei. *Atmospheric Chemistry and Physics*, *13*(17), 8879–8914. https://doi.org/10.5194/acp-13-8879-2013

Liao, J., Wolfe, G. M., Hannun, R. A., St. Clair, J. M., Hanisco, T. F., Gilman, J. B., et al. (2021). Formaldehyde evolution in US wildfire plumes during the Fire Influence on Regional to Global Environments and Air Quality experiment (FIREX-AQ). *Atmospheric Chemistry and Physics*, *21*(24), 18319–18331. https://doi.org/10.5194/acp-21-18319-2021

Lonsdale, C. R., Alvarado, M. J., Hodshire, A. L., Ramnarine, E., & Pierce, J. R. (2020). Simulating the forest fire plume dispersion, chemistry, and aerosol formation using SAM-ASP version 1.0. *Geoscientific Model Development*, *13*(9), 4579–4593. https://doi.org/10.5194/gmd-13-4579-2020

Lyapustin, A., Wang, Y., Korkin, S., Kahn, R., & Winker, D. (2020). MAIAC thermal technique for smoke injection height from MODIS. *IEEE Geoscience and Remote Sensing Letters*, *17*(5), 730–734. https://doi.org/10.1109/LGRS.2019.2936332

Mardi, A. H., Dadashazar, H., MacDonald, A. B., Braun, R. A., Crosbie, E., Xian, P., et al. (2018). Biomass burning plumes in the vicinity of the California coast: Airborne characterization of physicochemical properties, heating rates, and spatiotemporal features. *Journal of Geophysical Research: Atmospheres*, *123*(23), 13560–13582. https://doi.org/10.1029/2018JD029134

May, A. A., Lee, T., McMeeking, G. R., Akagi, S., Sullivan, A. P., Urbanski, S., et al. (2015). Observations and analysis of organic aerosol evolution in some prescribed fire smoke plumes. *Atmospheric Chemistry and Physics*, *15*(11), 6323–6335. https://doi.org/10.5194/acp-15-6323-2015

May, A. A., Levin, E. J. T., Hennigan, C. J., Riipinen, I., Lee, T., Collett, J. L., Jr., et al. (2013). Gas-particle partitioning of primary organic aerosol emissions: 3. Biomass burning. *Journal of Geophysical Research: Atmospheres*, *118*(19), 11327–11338. https://doi.org/10.1002/jgrd.50828

McClure, C. D., Lim, C. Y., Hagan, D. H., Kroll, J. H., & Cappa, C. D. (2020). Biomass-burning-derived particles from a wide variety of fuels – Part 1: Properties of primary particles. *Atmospheric Chemistry and Physics*, *20*(3), 1531–1547. https://doi.org/10.5194/acp-20-1531-2020

Moore, R. H., Wiggins, E. B., Ahern, A. T., Zimmerman, S., Montgomery, L., Campuzano Jost, P., et al. (2021). Sizing response of the ultra-high sensitivity aerosol spectrometer (UHSAS) and laser aerosol spectrometer (LAS) to changes in submicron aerosol composition and refractive index. *Atmospheric Measurement Techniques*, *14*(6), 4517–4542. https://doi.org/10.5194/amt-14-4517-2021

Morrison, H., Curry, J. A., & Khvorostyanov, V. I. (2005). A new double-moment microphysics parameterization for application in cloud and climate models. Part I: Description. *Journal of the Atmospheric Sciences*, *62*(6), 1665–1677. https://doi.org/10.1175/jas3446.1

O'Dell, K., Bilsback, K., Ford, B., Martenies, S. E., Magzamen, S., Fischer, E. V., & Pierce, J. R. (2021). Estimated mortality and morbidity attributable to smoke plumes in the United States: Not just a western US problem. *GeoHealth*, *5*(9), e2021GH000457. https://doi.org/10.1029/2021GH000457

O'Dell, K., Ford, B., Fischer, E. V., & Pierce, J. R. (2019). Contribution of wildland-fire smoke to US $PM_{2.5}$ and its influence on recent trends. *Environmental Science and Technology*, *53*(4), 1797–1804. https://doi.org/10.1021/acs.est.8b05430

Pagonis, D., Campuzano-Jost, P., Guo, H., Day, D. A., Schueneman, M. K., Brown, W. L., et al. (2021). Airborne extractive electrospray mass spectrometry measurements of the chemical composition of organic aerosol. *Atmospheric Measurement Techniques*, *14*(2), 1545–1559. https://doi.org/10.5194/amt-14-1545-2021

Pagonis, D., Selimovic, V., Campuzano-Jost, P., Guo, H., Day, D. A., Schueneman, M. K., et al. (2023). Impact of biomass burning organic aerosol volatility on smoke concentrations downwind of fires. *Environmental Science and Technology*, *57*(44), 17011–17021. https://doi.org/10.1021/acs.est.3c05017

Palm, B. B., Peng, Q., Fredrickson, C. D., Lee, B. H., Garofalo, L. A., Pothier, M. A., et al. (2020). Quantification of organic aerosol and brown carbon evolution in fresh wildfire plumes. *Proceedings of the National Academy of Sciences*, *117*(47), 29469–29477. https://doi.org/10.1073/pnas.2012218117

Palm, B. B., Peng, Q., Hall, S. R., Ullmann, K., Campos, T. L., Weinheimer, A., et al. (2021). Spatially resolved photochemistry impacts emissions estimates in fresh wildfire plumes. *Geophysical Research Letters*, *48*(23), e2021GL095443. https://doi.org/10.1029/2021GL095443

Peng, Q., Palm, B. B., Melander, K. E., Lee, B. H., Hall, S. R., Ullmann, K., et al. (2020). HONO emissions from western U.S. Wildfires provide dominant radical source in fresh wildfire smoke. *Environmental Science and Technology*, *54*(10), 5954–5963. https://doi.org/10.1021/acs.est.0c00126

Ramnarine, E., Kodros, J. K., Hodshire, A. L., Lonsdale, C. R., Alvarado, M. J., & Pierce, J. R. (2019). Effects of near-source coagulation of biomass burning aerosols on global predictions of aerosol size distributions and implications for aerosol radiative effects. *Atmospheric Chemistry and Physics*, *19*(9), 6561–6577. https://doi.org/10.5194/acp-19-6561-2019

Reid, J. S., & Hobbs, P. V. (1998). Physical and optical properties of young smoke from individual biomass fires in Brazil. *Journal of Geophysical Research*, *103*(D24), 32013–32030. https://doi.org/10.1029/98JD00159

Reid, J. S., Koppmann, R., Eck, T. F., & Eleuterio, D. P. (2005). A review of biomass burning emissions part II: Intensive physical properties of biomass burning particles. *Atmospheric Chemistry and Physics*, *27*.

Rémy, S., Veira, A., Paugam, R., Sofiev, M., Kaiser, J. W., Marenco, F., et al. (2017). Two global data sets of daily fire emission injection heights since 2003. *Atmospheric Chemistry and Physics*, *17*(4), 2921–2942. https://doi.org/10.5194/acp-17-2921-2017

Robinson, A. L., Donahue, N. M., Shrivastava, M. K., Weitkamp, E. A., Sage, A. M., Grieshop, A. P., et al. (2007). Rethinking organic aerosols: Semivolatile emissions and photochemical aging. *Science*, *315*(5816), 1259–1262. https://doi.org/10.1126/science.1133061

Ryerson, T. B., Williams, E. J., & Fehsenfeld, F. C. (2000). An efficient photolysis system for fast-response NO_2 measurements. *Journal of Geophysical Research*, *105*(D21), 26447–26461. https://doi.org/10.1029/2000JD900389

Sakamoto, K. M., Allan, J. D., Coe, H., Taylor, J. W., Duck, T. J., & Pierce, J. R. (2015). Aged boreal biomass-burning aerosol size distributions from BORTAS 2011. *Atmospheric Chemistry and Physics*, *15*(4), 1633–1646. https://doi.org/10.5194/acp-15-1633-2015

Sakamoto, K. M., Laing, J. R., Stevens, R. G., Jaffe, D. A., & Pierce, J. R. (2016). The evolution of biomass-burning aerosol size distributions due to coagulation: Dependence on fire and meteorological details and parameterization. *Atmospheric Chemistry and Physics*, *16*(12), 7709–7724. https://doi.org/10.5194/acp-16-7709-2016

Schill, G. P., Froyd, K. D., Bian, H., Kupc, A., Williamson, C., Brock, C. A., et al. (2020). Widespread biomass burning smoke throughout the remote troposphere. *Nature Geoscience*, *13*(6), 422–427. https://doi.org/10.1038/s41561-020-0586-1

Seinfeld, J. H., & Pandis, S. N. (2016). *Atmospheric chemistry and physics: From air pollution to climate change*. John Wiley and Sons, Incorporated. Retrieved from http://ebookcentral.proquest.com/lib/csu/detail.action?docID=4462549

Sekimoto, K., Koss, A. R., Gilman, J. B., Selimovic, V., Coggon, M. M., Zarzana, K. J., et al. (2018). High- and low-temperature pyrolysis profiles describe volatile organic compound emissions from western US wildfire fuels. *Atmospheric Chemistry and Physics*, *18*(13), 9263–9281. https://doi.org/10.5194/acp-18-9263-2018

Shetter, R. E., & Müller, M. (1999). Photolysis frequency measurements using actinic flux spectroradiometry during the PEM-Tropics mission: Instrumentation description and some results. *Journal of Geophysical Research*, *104*(D5), 5647–5661. https://doi.org/10.1029/98JD01381

Shrivastava, M., Cappa, C. D., Fan, J., Goldstein, A. H., Guenther, A. B., Jimenez, J. L., et al. (2017). Recent advances in understanding secondary organic aerosol: Implications for global climate forcing. *Reviews of Geophysics*, *55*(2), 509–559. https://doi.org/10.1002/2016RG000540

Shrivastava, M., Fan, J., Zhang, Y., Rasool, Q. Z., Zhao, B., Shen, J., et al. (2024). Intense formation of secondary ultrafine particles from Amazonian vegetation fires and their invigoration of deep clouds and precipitation. *One Earth*, *7*(6), 1029–1043. https://doi.org/10.1016/j.oneear.2024.05.015

Smith, J. D., Sio, V., Yu, L., Zhang, Q., & Anastasio, C. (2014). Secondary organic aerosol production from aqueous reactions of atmospheric phenols with an organic triplet excited state. *Environmental Science and Technology*, *48*(2), 1049–1057. https://doi.org/10.1021/es4045715

Spracklen, D. V., Carslaw, K. S., Pöschl, U., Rap, A., & Forster, P. M. (2011). Global cloud condensation nuclei influenced by carbonaceous combustion aerosol. *Atmospheric Chemistry and Physics*, *11*(17), 9067–9087. https://doi.org/10.5194/acp-11-9067-2011

Stockwell, C. E., Veres, P. R., Williams, J., & Yokelson, R. J. (2015). Characterization of biomass burning emissions from cooking fires, peat, crop residue, and other fuels with high-resolution proton-transfer-reaction time-of-flight mass spectrometry. *Atmospheric Chemistry and Physics*, *15*(2), 845–865. https://doi.org/10.5194/acp-15-845-2015

Vakkari, V., Kerminen, V.-M., Beukes, J. P., Tiitta, P., van Zyl, P. G., Josipovic, M., et al. (2014). Rapid changes in biomass burning aerosols by atmospheric oxidation. *Geophysical Research Letters*, *41*(7), 2644–2651. https://doi.org/10.1002/2014GL059396

Wallace, J. M., & Hobbs, P. V. (2006). *Atmospheric science: An introductory survey*. Elsevier.

Walter, C., Freitas, S. R., Kottmeier, C., Kraut, I., Rieger, D., Vogel, H., & Vogel, B. (2016). The importance of plume rise on the concentrations and atmospheric impacts of biomass burning aerosol. *Atmospheric Chemistry and Physics*, *16*(14), 9201–9219. https://doi.org/10.5194/acp-16-9201-2016

Wang, S., Coggon, M. M., Gkatzelis, G. I., Warneke, C., Bourgeois, I., Ryerson, T., et al. (2021). Chemical tomography in a fresh wildland fire plume: A large eddy simulation (LES) study. *Journal of Geophysical Research: Atmospheres*, *126*(18), e2021JD035203. https://doi.org/10.1029/2021JD035203

Warneke, C., Schwarz, J. P., Dibb, J., Kalashnikova, O., Frost, G., Al-Saad, J., et al. (2023). Fire influence on regional to global environments and air quality (FIREX-AQ). *Journal of Geophysical Research: Atmospheres*, *128*(2), e2022JD037758. https://doi.org/10.1029/2022JD037758

Washenfelder, R. A., Azzarello, L., Ball, K., Brown, S. S., Decker, Z. C. J., Franchin, A., et al. (2022). Complexity in the evolution, composition, and spectroscopy of Brown carbon in aircraft measurements of wildfire plumes. *Geophysical Research Letters*, *49*(9), e2022GL098951. https://doi.org/10.1029/2022GL098951

Wiedinmyer, C., Akagi, S. K., Yokelson, R. J., Emmons, L. K., Al-Saadi, J. A., Orlando, J. J., & Soja, A. J. (2011). The fire INventory from NCAR (FINN): A high resolution global model to estimate the emissions from open burning. *Geoscientific Model Development*, *4*(3), 625–641. https://doi.org/10.5194/gmd-4-625-2011

Xu, L., Crounse, J. D., Vasquez, K. T., Allen, H., Wennberg, P. O., Bourgeois, I., et al. (2021). Ozone chemistry in western U.S. wildfire plumes. *Science Advances*, *7*(50), eabl3648. https://doi.org/10.1126/sciadv.abl3648

Yokelson, R. J., Crounse, J. D., DeCarlo, P. F., Karl, T., Urbanski, S., Atlas, E., et al. (2009). Emissions from biomass burning in the Yucatan. *Atmospheric Chemistry and Physics*, *9*(15), 5785–5812. https://doi.org/10.5194/acp-9-5785-2009

Yue, X., Mickley, L. J., Logan, J. A., & Kaplan, J. O. (2013). Ensemble projections of wildfire activity and carbonaceous aerosol concentrations over the western United States in the mid-21st century. *Atmospheric Environment*, *77*, 767–780. https://doi.org/10.1016/j.atmosenv.2013.06.003

Zhou, S., Collier, S., Jaffe, D. A., Briggs, N. L., Hee, J., Sedlacek III, A. J., et al. (2017). Regional influence of wildfires on aerosol chemistry in the western US and insights into atmospheric aging of biomass burning organic aerosol. *Atmospheric Chemistry and Physics*, *17*(3), 2477–2493. https://doi.org/10.5194/acp-17-2477-2017